Available online at www.sciencedirect.com
ScienceDirect
Geochimica et Cosmochimica Acta 71 (2007) 4974–4996
Geochimica et Cosmochimica Acta
www.elsevier.com/locate/gca

Mobilization of Ti–Nb–Ta during subduction: Evidence from rutile-bearing dehydration segregations and veins hosted in eclogite, Tianshan, NW China

Jun Gao [a], Timm John [b,c,*], Reiner Klemd [d], Xianming Xiong [a]

[a] Key Laboratory of Mineral Resources, Institute of Geology and Geophysics, Chinese Academy of Sciences, P.O. Box 9825, Beijing 100029, China
[b] Physics of Geological Processes PGP, University of Oslo, P.O. Box 1048 Blindern, 0316 Oslo, Norway
[c] Institut für Geowissenschaften and SFB 574, Universität Kiel, Olshausenstr. 40, 24098 Kiel, Germany
[d] Mineralogisches Institut, Universität Würzburg, Am Hubland 97074, Würzburg, Germany

Received 14 February 2007; accepted in revised form 19 July 2007; available online 7 September 2007

Abstract

Field evidence from the western Tianshan subduction complex in northwestern China indicates that the high field strength elements Ti, Nb, and Ta were mobilized and thereby fractionated from Zr and Hf during the dehydration process that transformed blueschist into eclogite. Both a segregation with a depletion halo, thought to represent initial mobilization during dehydration, and a transport vein, indicative of the long distance transport were investigated. In each case, centimeter-sized rutile grains grew as needle-like crystals in the segregation and as prismatic crystals in the vein. Within the host rock of the segregation, the Ti contents of garnet and omphacite, the modal abundances of rutile and titanite and the bulk rock Ti, Nb, and Ta contents decrease towards the segregation. These observations are consistent with transport of Ti, Nb, and Ta from the host rock into the segregation. Textural and geochemical data for the eclogite-facies vein minerals indicate that Ti–Nb–Ta-rich fluids were transported over long-distances (at minimum meter-scale) during fracture-controlled fluid flow. Complex forming ligands (e.g., Na–Si–Al polymers and F^-) may have enhanced the solubility of Ti, Nb, and Ta in the fluid. Changes in fluid composition (e.g., X_{CO_2}) may both precipitate rutile and fractionate Ti, Nb, and Ta from LILE and REE.

1. INTRODUCTION

Calc-alkaline volcanic rocks situated along convergent plate margins are enriched in large ion lithophile elements (LILE) and depleted in high field strength elements (HFSE). The genesis of these rocks has been attributed to the melting of the mantle wedge, triggered by the influx of subduction-zone fluids (e.g., Tatsumi, 1989; McCulloch and Gamble, 1991). This distinct geochemical signature is thought to result from dehydration with retention of rutile in subducted slabs (e.g., Ryerson and Watson, 1987; Scambelluri and Philippot, 2001; Tropper and Manning, 2005). Thus, rutile controls the HFSE content of fluid released during the devolatilization of subducting oceanic lithosphere (Brenan et al., 1994; Ayers, 1998). The low solubility of rutile in H_2O (Audetat and Keppler, 2005; Tropper and Manning, 2005) and the large partition coefficients for Ti, Nb, and Ta (Brenan et al., 1994; Stalder et al., 1998) between rutile and the fluid support this model. However, the presence of rutile or zircon as vein minerals in deeply subducted rocks (e.g., Selverstone et al., 1992; Franz et al., 2001; Rubatto and Hermann, 2003) and as daughter minerals in fluid inclusions in eclogitic omphacite (e.g., Philippot and Selverstone, 1991) indicates that HFSE may be both soluble and transportable during fluid flow within deep regions of subduction zones. Metasomatic

* Corresponding author. Fax: +47 22 85 51 01.
E-mail addresses: gaojun@mail.igcas.ac.cn (J. Gao), timm.john@ fys.uio.no (T. John), reiner.klemd@mail.uni-wuerzburg.de (R. Klemd).

0016-7037/$ - see front matter © 2007 Elsevier Ltd. All rights reserved.
doi:10.1016/j.gca.2007.07.027

fluids have been interpreted to be extremely effective in transporting and enriching HFSE in the HP-terranes (e.g., Sorensen and Grossman, 1989; Bröcker and Enders, 2001; John et al., 2007).

Both the decoupling of water and trace element release in subducted oceanic crust, and the inability of trace element transfer to the mantle wedge via aqueous fluids have also been proposed (Hermann et al., 2006). The authors suggest, based on experimental data and field evidence, that aqueous fluids are too dilute to be a likely agent for the required trace element transport. Therefore, both the role of rutile partitioning in subduction zone fluids and the composition of subduction fluids pose fundamental dilemmas in understanding the geochemical characteristics of island-arc volcanic rocks. A supercritical fluid with melt-like solubilities of HFSE has been suggested to act as a carrier medium for trace elements between the slab and the mantle wedge (Stolper and Newman, 1994; Kessel et al., 2005; Hermann et al., 2006): however, the temperature and pressure conditions necessary to create such a fluid are much higher than those reported for the dominant subduction zone fluid release process in the oceanic crust, namely, at conditions of the blueschist to eclogite transition (Peacock, 1993; Schmidt and Poli, 1998). A major pulse of fluid release occurs as wet blueschist (4 to 5 wt% fluid) transforms to dry eclogite (<1 wt% fluid), at 50 to 70 km depths (Peacock, 1993). Some have concluded that almost all this fluid, stored in the oceanic crust and the upper part of the hydrated slab mantle, would leave the slab without almost any chemical effects (e.g., Hermann et al., 2006), whereas others point out the reactivity of the released aqueous fluids while traveling through the slab towards the mantle wedge (Zack and John, 2007). In addition, Feineman et al. (2007) suggested that the initial fluid composition as derived during slab dehydration would be changed by the mixing with the partial melts of the sediment layer and the exchange with the mantle wedge.

Veins produced at eclogite-facies conditions within subducted oceanic lithosphere are interpreted to represent former fluid pathways within the slab and thus are thought to reflect how such fluids interact with rocks during flow (e.g., Becker et al., 1999; Gao and Klemd, 2001; Scambelluri et al., 2001; John and Schenk, 2003, 2006; John et al., 2007). In this paper, we report petrological and geochemical data from two localities, an eclogite-facies rutile-bearing segregation and a rutile vein from the Tianshan Mts. of NW China, in order to evaluate cm- to m-scale transport of the traditionally "fluid immobile" HFSE Nb, Ta, and Ti.

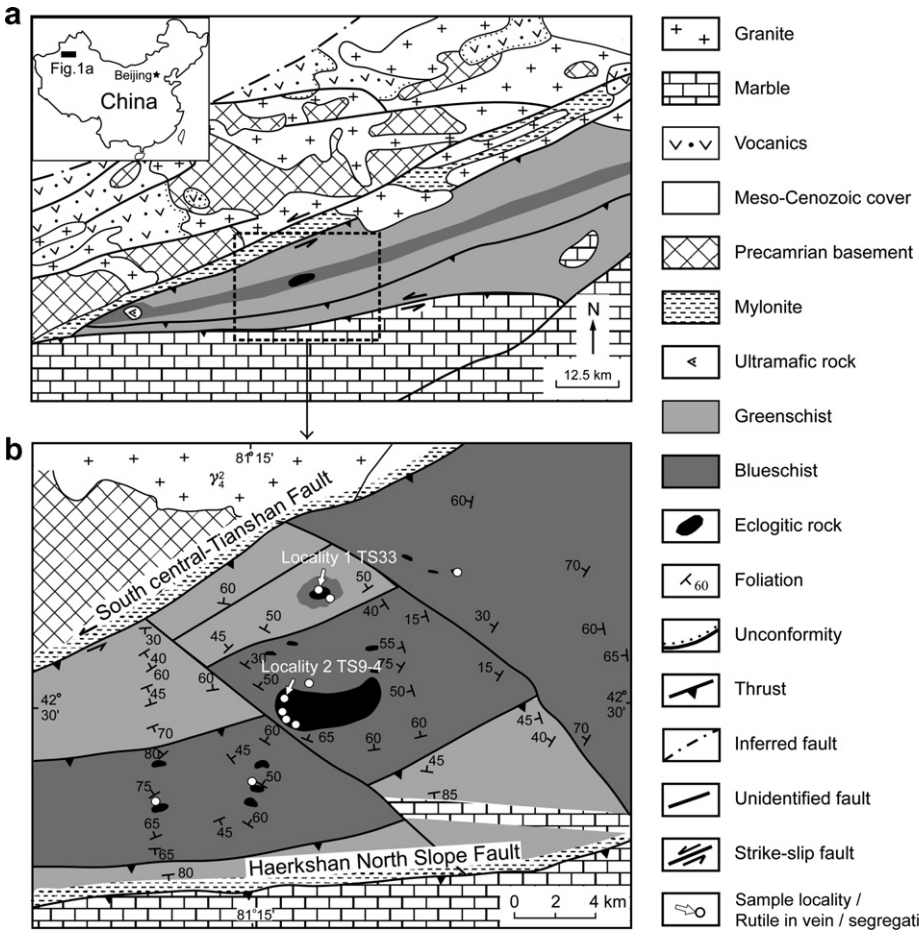

Fig. 1. Schematic tectonic map of the western Tianshan high-pressure low-temperature metamorphic belt in northwestern China. (a) Local geological map; (b) Detailed geological map showing the distribution of rutile-bearing segregations and veins and the localities of the samples TS33 (segregation) and TS9-4 (vein).

2. GEOLOGICAL CONTEXT

Networks of eclogite-facies veins derived from the dehydration of blueschists are present in the western Tianshan high-pressure low-temperature metamorphic belt in northwestern China (Gao et al., 1998; Gao and Klemd, 2001; Fig. 1). The vein-bearing unit is mainly composed of blueschist-, eclogite-, and greenschist-facies metasedimentary

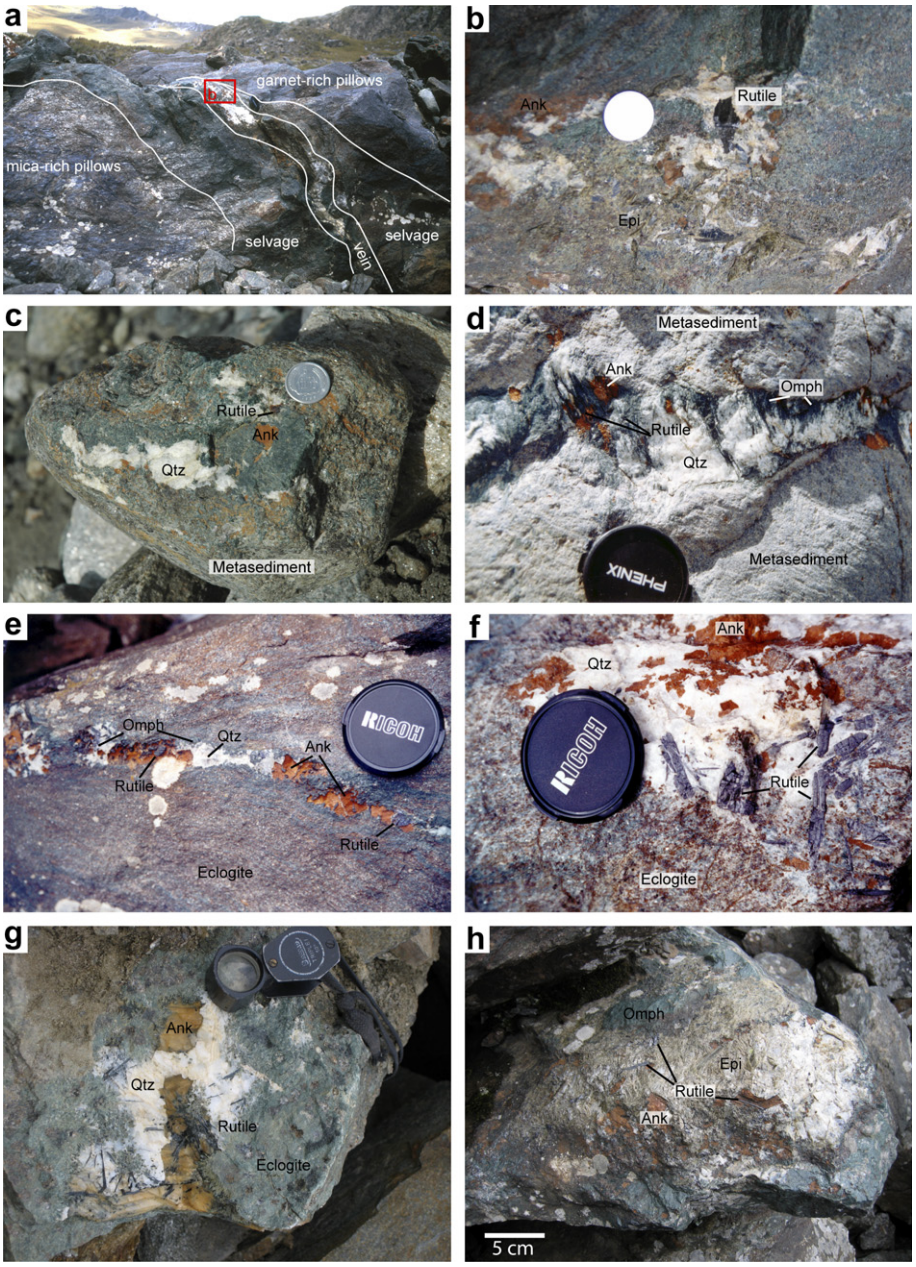

Fig. 2. (a) A vein with reaction selvage cuts through two, compositionally different blueschist pillow-sequences. (b) Close up of (a) shows cm size rutile associated with ankerite, quartz, and epidote. (c) A vein consisting of omphacite, quartz, ankerite, and rutile cuts a pelitic metasediment. (d) A vein consisting of omphacite, quartz, ankerite, and rutile cuts a quartzitic metasediment. (e) Eclogite with rutile-bearing vein. Again, rutile is associated with quartz, omphacite, and ankerite. (f–h) Rutile-bearing segregations in eclogites. Large rutiles associated with quartz, ankerite, omphacite, and epidote. (i–k) An oriented acicular rutile-bearing segregation occurs in the center of an eclogite boudin enclosed by blueschist. TS33-5A, TS33-5B, and TS33-2 are samples collected from the eclogite boudin. (j) Orientated acicular rutile segregation in the center of an eclogite boudin within blueschist indicating the growth of rutile in a fluid-filled cavity under peak eclogite-facies conditions. (Sample TS33-5B). (k) Fibrous omphacites and rutiles in the segregation close to the host eclogite; (a–e) mark the whole rock samples taken for chemical composition analysis along a profile with varying distance to the segregation. (l) A high-pressure vein, composed of ca. 50% omphacite, 2% amphibole, 0.5% phengite, 21% quartz, 1.5% ankerite, 5% apatite, and 20% rutile (Sample TS9-4), cuts the foliated host eclogite with a sharp interface, indicating the externally derived transport character of this vein.

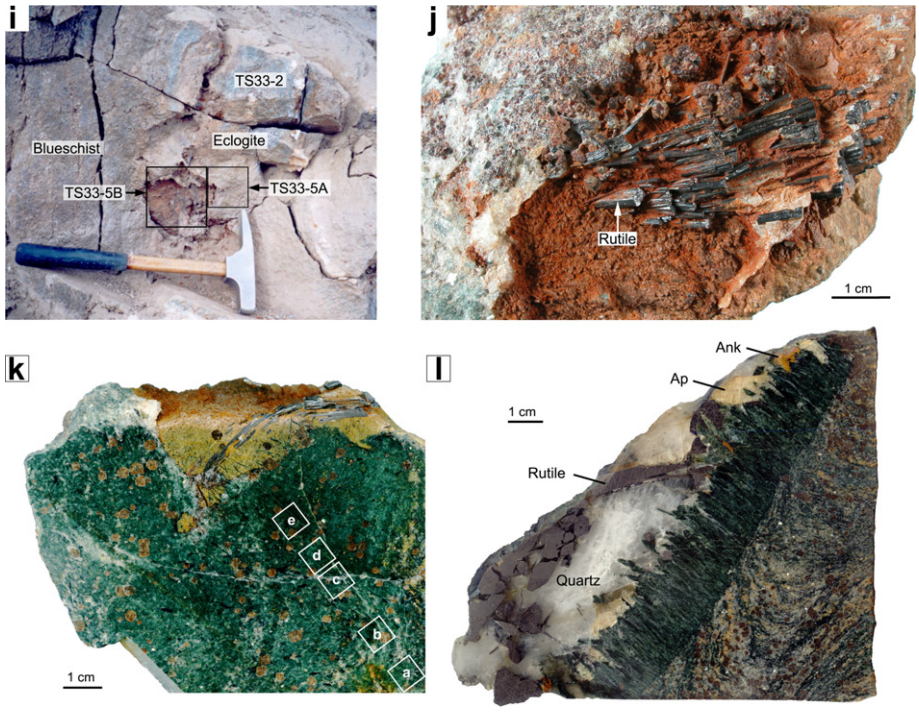

Fig. 2 (*continued*)

rocks and some mafic metavolcanic rocks (Gao et al., 1995; Gao et al., 1999; Gao and Klemd, 2003). The trace-element compositions of the mafic rocks are similar to those of depleted to enriched mid-ocean ridge, ocean island and arc related basalts (Gao and Klemd, 2003; John et al., 2007). Blueschist occurs within greenschist-facies metasediments as small discrete bodies, lenses, bands and as up to 4 km-thick layers (Fig. 1). Eclogites are interlayered with the blueschist layers as pods (15 to 25 cm in diameter), boudins (0.2×0.5 to 5×20 m^2), layers (2 to 50 cm thick) or as a massive block (almost 2 km^2 in plan view). The latter is not only composed of eclogite, but also of omphacitite, epidosite, and omphacite-bearing blueschist, and is cut by eclogite-facies vein networks. The transition between blueschist and eclogite is locally gradual, and both underwent prograde conditions of 480 to 580 °C at 1.9 to 2.1 GPa (e.g., Klemd et al., 2002; Wei et al., 2003). Sm–Nd isochron data (Omp–Gln–Grt-whole rock) of 343 ± 44 Ma and a well-defined $^{40}Ar/^{39}Ar$ age of 344 ± 1 Ma for crossite suggest a Carboniferous age for the peak of metamorphism (Gao and Klemd, 2003). White mica geochronology (K–Ar, Ar–Ar, Rb–Sr) supplies ages clustering at 310 Ma, interpreted to date exhumation (Klemd et al., 2005).

The vein network in the Tianshan HP-rocks appears to consist of both locally derived dehydration segregations and veins and externally derived transport veins, see John et al. (2007) for definitions and Gao and Klemd (2001) for a detailed description. A striking feature of this vein system is that segregations and veins occasionally contain up to 10 cm sized rutile grains (Fig. 2), usually associated with omphacite, quartz and ankerite but also with epidote minerals and minor garnet. The veins, consisting of these typical and uniform mineral assemblages, cut through all lithologies, i.e., eclogites, blueschists, and high-pressure quartzitic and metapelitic rocks (Fig. 2), indicating that transport was not limited to the dehydrating blueschists.

3. SAMPLE DESCRIPTION AND PETROGRAPHY

3.1. Locality 1, segregation hosted in eclogite boudin

Oriented, acicular centimeter-sized rutile crystals occur as inclusions in ankerite in an irregularly shaped segregation in the centre of an eclogite boudin, which itself is enclosed by blueschist (Sample TS33-5B; Fig. 1b and Fig. 2i–k). The segregation also contains garnet, omphacite and quartz with minor apatite, phengite and amphibole (Table 1). The segregation displays a sharp contact with the host eclogite and the rutile needles and omphacite fibers occur perpendicular to the wall of the segregation (Fig. 2j and k). The modal amounts of minerals in the segregation are 5% Grt, 5% Omp, 0.4% Amp, 0.1% Ph, 0.4% Pg, 15% Qtz, 43% Ank, 0.1% Ap, 1% Ttn, and 30% Rt. However, due to the erosion or removal of ankerite, which may have contained several other minerals, this estimate may have a large uncertainty. Garnet 1 (garnet in the segregation) is either inclusion free or contains omphacite inclusions. The host eclogite consists of garnet 2 (garnet in the host eclogite), omphacite, paragonite, and rutile and/or titanite, along with minor zoisite, apatite, and carbonate (Table 1). Rare glaucophane porphyroblasts, which typically contain inclusions of omphacite, likely formed at the latter mineral's expense. Garnet 2 contains inclusions of zoisite, paragonite, glaucophane, carbonate, and titanite (Fig. 3a). Fine-grained (<15 μm) zircons occur well distributed in the host eclogite and as inclusions in rutile, apatite and garnet (Fig. 3b and d).

Table 1
Modal abundances of minerals in the segregation, the host eclogite of the segregation, the vein and the host eclogite

Sample:	Grt	Omp	Amp	Zo	Ph	Pg	Qtz	Ank	Ap	Rt	Ttn	Zr
Segregation TS33-5B:	5	5	0.4	—	0.1	0.4	15	43	0.1	30	1	—
Host eclogites of the segregation												
TS33-5A	20	65	2	1	—	8	1	1	0.5	0.5	1	<0.1
TS33-5B	15	70	3	1	—	8	0.8	0.4	0.3	0.5	1	<0.1
TS33-2	37	45	2	1	—	10	3.8	0.3	0.1	0.3	0.5	<0.1
TS33-5B-a	16	70	0.5	1	—	10	0.4	0.5	0.1	0.5	1	<0.1
TS33-5B-b	16	70	0.2	1	—	10	1	0.5	0.1	0.4	0.8	<0.1
TS33-5B-c	15	70	1	0.5	—	10	2	0.5	0.1	0.3	0.6	<0.1
TS33-5B-d	10	75	1	0.5	—	11.25	0.7	0.5	0.3	0.25	0.5	<0.1
TS33-5B-e	7.5	75	—	0.5	—	12	0.3	3	1	0.2	0.4	<0.1
Vein												
TS9-4	—	50	2	—	0.5	—	21	1.5	5	20	—	—
Host eclogites of the vein												
TS9-4	20	40	10	2	10	5	—	5	—	2	6	<0.1

Titanite and rutile have variable grain sizes, but are usually homogenously distributed throughout the host eclogite. Titanite typically occurs as helicitic porphyroblasts or as inclusions in rutile (Fig. 3c). Both the titanite and rutile tend to form fine-grained xenomorphic clusters (Fig. 3c). The modal amounts of titanite and/or rutile in the host eclogite decrease drastically from ~1.5 to ~0.5 vol% over ten centimeters towards the segregation (Table 1). Primary, tubular two- to three-phase, fluid inclusions were entrapped in both fibrous omphacite grains and in omphacite inclusions in garnet from the segregation (Fig. 4a and b), as well as in matrix omphacite of the host eclogite (Fig. 4c). The blueschist host of the eclogite boudin is composed of garnet, glaucophane, calcic-amphibole, phengite, paragonite, albite, ankerite, and titanite. Omphacite and rutile inclusions in garnet and glaucophane, the latter of which is rimmed by calcic amphibole, suggest the blueschist is retrogressed eclogite. This is further supported by glaucophane and omphacite inclusions in albite porphyroblasts within the blueschist.

3.2. Locality 2, vein in eclogite

A vein that consists of omphacite, rutile, quartz, apatite, ankerite, and minor glaucophane, barroisite, and phengite was found in eclogite (TS9-4; Figs. 1b and 2l). This ~10 centimeter-wide vein can be traced for a length of almost 10 m across an outcrop, which is the minimum length of this vein since its full extent is not exposed (i.e., the start and the end). The vein cuts the foliation of the host eclogite: the interface between vein and host is both sharp and lacks a "transition zone" or "vein envelope" (see John et al., 2007 for definition). In the vein, centimeter-sized fibrous omphacite grew perpendicular (syntaxially) from the vein wall to the median line, whereas centimeter-sized rutile prisms are typically randomly oriented. The fibrous omphacite grains generally contain dark irregular cores surrounded by lighter-colored rims (Fig. 3e). The cores display inclusions of quartz and more rarely albite, which indicates that the reaction Ab = Jd + Qtz remained uncompleted (Fig. 3f). Some centimeter-sized apatite grains and minor ankerite are intergrown with the omphacite fibers and rutile prisms. Fine-grained omphacite also occurs as inclusions in apatite (Fig. 2l). The estimated modal amounts of minerals in the vein (Sample TS9-4) are 50% Omp, 2% Amp, 0.5% Ph, 21% Qtz, 1.5% Ank, 5% Ap, and 21% Rt. No variations of the mineral modal contents towards the vein have been observed in the vein's host eclogite, throughout the investigated parts they are ca. 20% Grt, 40% Omp, 10% Amp, 10% Ph, 5% Pg, 5% Ank, 2% Rt, and 6% Ttn (Table 1). The host eclogite contains garnet porphyroblasts with inclusions of zoisite, paragonite, glaucophane, omphacite, carbonate, and rutile. Orientated omphacite, phengite, and paragonite crystals define the foliation of the host eclogite. Fine-grained (<15 μm) zircons are equally distributed in the rock and were detected as inclusions in titanite and phengite crystals. Tubular two- to three-phase aqueous fluid inclusions that contain liquid, a gas bubble ± a crystal of calcite or siderite were observed in both the core and the rim of the fibrous vein omphacite (Fig. 4d–f).

4. ANALYTICAL METHODS

Doubly polished thin sections of about 0.25 mm in thickness were prepared for the microthermometric study. Fluid inclusions were examined using the LINKAM-TMS94 gas-flow-heating/freezing stage at the China University of Geosciences (Beijing). The stage was calibrated using synthetic fluid standards (Syn Flinc, Inc.), which have known phase transitions at −56.6, 0, and 374.1 °C. The precision is +0.2 °C for the final meting temperature (Tmf) and ±1 °C for the homogenization temperature (Th). The used heating rate is about 0.1 °C/min for Tmf and 3.0 °C/min for Th. Laser-Raman spectroscopy was performed at the Institute of Geology and Geophysics, Chinese Academy of Sciences in Beijing using a Renishaw Raman MKI-1000 system equipped with a CCD detector and an Ar ion laser. The laser beam with a wavelength of 514.5 nm was focused on bubbles and daughter mineral crystals in fluid inclusions in omphacite through 50× and 100× objectives of a light

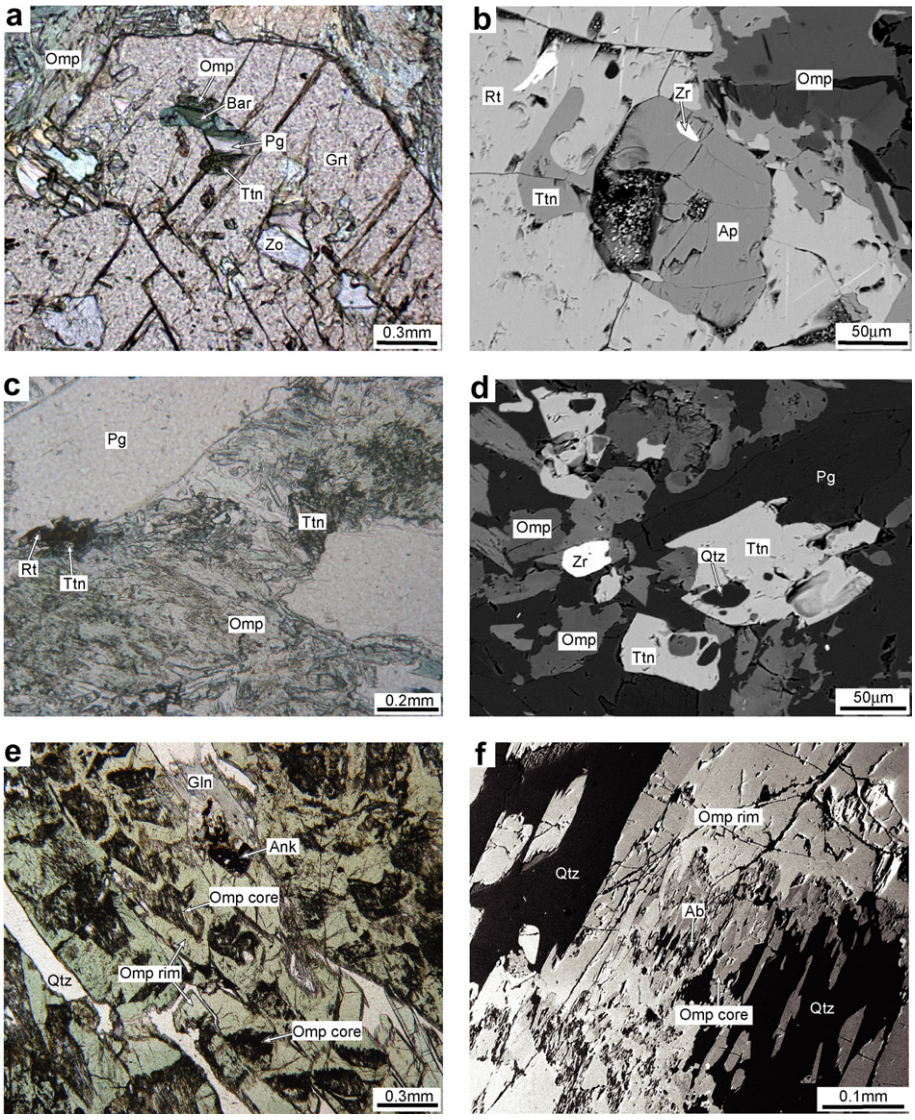

Fig. 3. Microphotographs showing textures for sample TS33-5B and TS9-4. (a) Garnet with prograde entrapped inclusions of the former blueschist facies mineral assemblage (TS33-5B). (b) Titanite, apatite, and zircon inclusion in large rutile (TS33-5B). (c) Fine-grained xenomorphic titanite and rutile clusters in segregation host eclogite (Plane light, TS33-5B). (d) The bse image of the matrix shows a mirco zircon in contact with omphacite. (e) Fibrous omphacite contains dark irregular cores rimmed by lighter-colored green rims (Plane light, Sample TS9-4 vein). (f) The core of fibrous omphacite is composed of omphacite, quartz, and sparse albite; the back scattered electron image of fibrous omphacite shows the constituents of the core and rim.

microscope. The laser spot size was focused to 1 μm. The reproduction of spectra for the same spot is better than 0.2 cm^{-1}.

The major and trace element compositions of whole rocks (samples TS33-5A, TS33-5B, TS33-2, and TS9-4host) were measured at the Institute of Mineralogy of the Universität Würzburg. The major element compositions were obtained by X-ray fluorescence analysis (XRF; PHILIPS PW1480) using fused glass disks. The trace elements were determined by laser ablation inductively-coupled plasma mass spectrometry (LA-ICP-MS; Agilent 7500i) on the same glass targets as used for XRF. Bulk rock concentrations of SiO_2 were used for normalization of LA-ICP-MS analyses. The glass reference material NIST SRM 612 was used for external calibration and calculation of trace element concentration by the GLITTER Version 3.0 online interactive data reduction for LA-ICP-MS Program by Macquarie Res. (2000). The analytical accuracy of this method is 10% or less for the trace elements as was shown in an interlaboratory programme, in which 65 laboratories (including ours) involving 16 independent analytical methods such as definitive (isotope dilution) and comparative bulk (e.g., INAA, ICPMS, and SSMS) and microanalytical (e.g., LA-ICPMS, SIMS, and EPMA) methods participated in the geochemical characterization of the MPI-DING glasses (Jochum et al., 2006). Furthermore, a comparison of bulk rock mean results from 5 extraction lines shows coincidence within 1σ error with the data from acid solution ICP-MS (Schulz et al., 2004), except for La. A certain amount of La was (<10 ppm) introduced with the $LiBO_4$

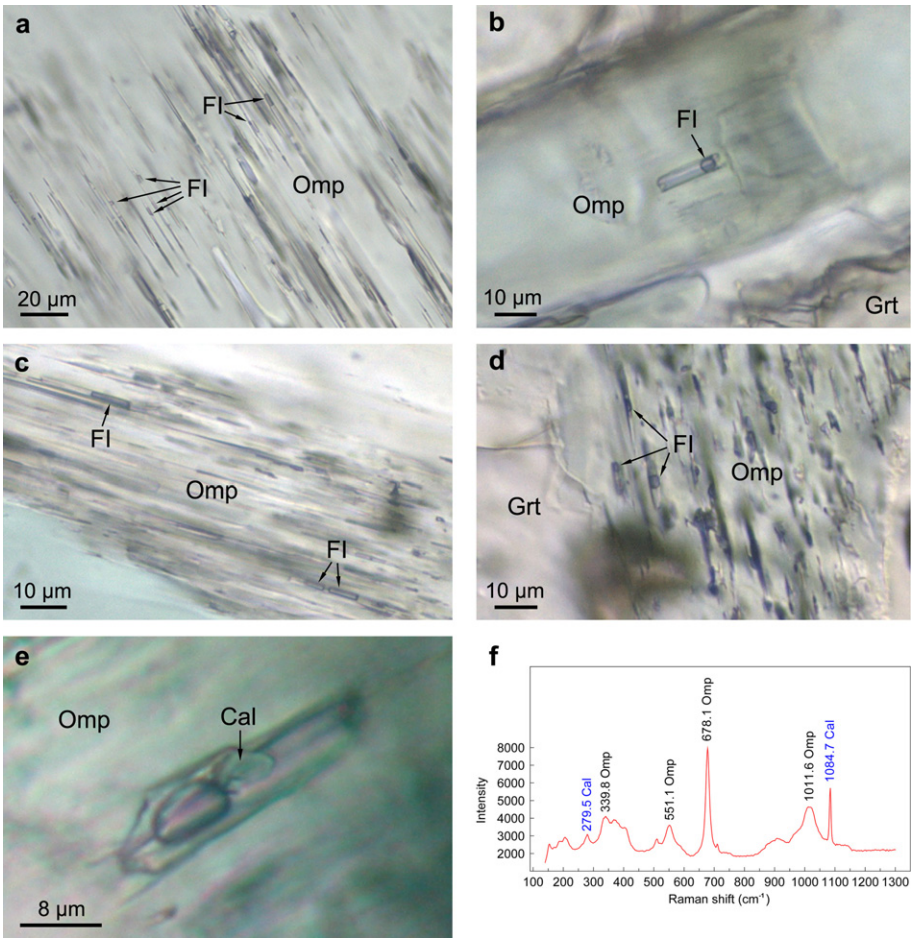

Fig. 4. Microphotographs showing primary fluid inclusions in omphacites. (a) Two-phase tubular fluid inclusions in fibrous omphacites growing across the contact of the segregation and the host, sample TS33-5B. (b) Two-phase tubular fluid inclusions in an omphacite inclusion in a garnet porphyroblast of the host eclogite, sample TS33-5B. (c) Two-phase tubular inclusions in matrix omphacites of the host eclogite, sample TS33-5B. (d) Two to three-phase tubular inclusions (liquid + bubble + calcite) in matrix omphacites of the host eclogite, sample TS9-4. (e) Primary two to three phase fluid inclusions (liquid + bubble ± calcite) preserved in omphacite fibers perpendicular to the vein border, Omp, omphacite; Cal, calcite. (f) Raman spectra of calcite in a primary fluid inclusion in fibrous omphacite, sample TS9-4, Omp, omphacite; Grt, garnet; Cal, calcite; FI, fluid inclusion.

flux into the glass beads and was empirically corrected by regression through comparison of samples with different La concentrations (Sylvester, 2003). In the here conducted study the analyses (Table 2) are the mean values of 5 scanned lines. The standard error for the individual samples (reproducibility) is <8% relative for the element concentrations >1 ppm, for element concentrations <1 ppm between 10% and 14% and the error for element concentrations <0.1 ppm can reach up to 20%. The accuracy of the measurements of the applied method was controlled by repeated analysis of NIST 614 and whole rock standards (BE-N Basalt, MAG-1 Marine Mud). Based on analysis of NIST SRM 614, the precision for REE, Nb, Ta, and Th is <8% (based on 1σ). For further details see Brätz and Klemd (2002). The major and trace element compositions of whole rock samples TS33-5B-a, b, c, d, e and TS9-4vein were measured at the Institut für Geowissenschaften, Universität Kiel. There, the major elements were measured by XRF (PHILIPS PW1480) on fused glass disks. The concentrations of trace elements were determined after $HF–HNO_3–HClO_4$ acid digestion in bombs at 180 °C of approximately 100 mg pulverized sample with an Agilent 7500c ICP mass spectrometry. The analytical precision is 10% or less for the trace elements. Further details of the sample preparation procedure and instrument calibration strategy for this analytical method can be found in Garbe-Schönberg (1993) and John et al. (2007).

The major and minor element compositions of silicate minerals and rutile were analyzed on a JEOL JXA 8100 Superprobe at the Department of Geology, Peking University, using an accelerating voltage of 15 kV, beam current of 1×10^{-8} A and spot diameter of 1 μm. Apatite analyses were performed on a JEOL 8900R electron microprobe at the Universität Kiel, equipped with five wavelength-dispersive spectrometers (WDS). For apatite analyses, the instrument is typically operated with a 10 kV acceleration voltage and a 15 nA beam. Sample spot sizes were ca. 10 μm. Citzaf (Armstrong, 1995) was used for the matrix correction of

Table 2
Bulk geochemical data, major and trace elements, of segregation, vein and their host eclogites

Sample:	TS33-5A	TS33-5B	TS33-2	TS33	TS33-5B-a	TS33-5B-b	TS33-5B-C	TS33-5B-d	TS33-5B-e	TS9-4-1	TS9-4-2
Location:	Host rocks of the segregation	Host rocks of the segregation	Host rocks of the segregation	Host rocks of the segregation average	Host (7.3 cm to the segregation)	Host (5.7 cm to the segregation)	Host (3.7 cm to the segregation)	Host (2.8 cm to the segregation)	Host (1.5 cm to the segregation)	Host rocks of the vein	Vein
Major elements (wt%)											
SiO_2	53.65	55.52	56.19	55.12	55.30	55.55	57.99	55.83	55.29	38.20	54.09
Al_2O_3	14.96	15.37	15.23	15.19	18.63	15.27	14.24	14.25	12.63	15.31	2.30
Fe_2O_3	6.51	7.29	10.85	8.22	7.40	8.87	6.54	7.32	6.35	12.52	2.37
MnO	0.06	0.06	0.15	0.09	0.08	0.09	0.04	0.06	0.04	0.14	0.01
MgO	4.80	4.63	3.84	4.42	6.34	8.06	9.00	9.26	10.08	4.13	4.35
CaO	9.36	8.48	7.59	8.48	3.37	4.18	4.93	5.07	5.40	12.73	1.19
Na_2O	5.62	6.55	4.87	5.68	5.83	5.83	6.81	6.51	7.02	3.62	2.26
P_2O_5	0.38	0.01	0.09	0.16	0.01	0.02	0.02	0.04	0.17	0.74	3.18
LOI	3.42	1.03	0.50	1.65	1.65	1.68	1.28	1.38	4.53	6.58	1.41
Total*	99.80	99.99	99.99	99.93	99.69	100.35	101.48	100.23	101.94	99.35	99.43
Trace elements (ppm)											
Pb	2.19	2.20	1.75	2.05	2.36	1.39	1.00	0.995	0.854	3.52	2.37
Sr	145	89.2	66.5	100	129	64.5	53.5	51.1	37.6	258	76.5
Cs	0.050	0.060	0.050	0.053	0.050	0.031	0.028	0.035	0.029	0.650	0.051
Ba	14.7	13.6	8.80	12.4	16.03	11.3	11.5	8.92	5.43	193	9.94
Rb	1.08	1.18	1.13	1.13	1.44	0.944	0.885	0.948	0.624	17.3	1.09
K_2O **	0.140	0.130	0.110	0.127	0.210	0.110	0.110	0.100	0.070	0.990	0.050
Th	1.12	0.930	0.881	0.976	0.402	0.586	0.379	0.352	0.442	2.16	0.009
U	0.470	0.386	0.461	0.439	0.206	0.273	0.229	0.229	0.266	0.900	0.057
TiO_2 **	0.900	0.92	0.570	0.797	0.870	0.690	0.520	0.410	0.360	4.39	28.2
Nb	3.07	3.42	1.81	2.77	2.87	2.22	1.42	1.14	1.02	36.2	184
Ta	0.240	0.252	0.138	0.210	0.196	0.156	0.112	0.088	0.078	2.14	12.9
Zr	97.6	83.7	68.1	83.1	74.7	81.7	98.2	112	124	303	5.42
Hf	2.79	2.36	1.83	2.33	2.23	2.43	2.93	3.24	3.63	6.91	0.277
Nb/Ta	**12.8**	**13.6**	**13.1**	**13.2**	**14.7**	**14.2**	**12.8**	**13.0**	**13.1**	**16.9**	**14.2**
Zr/Hf	**35.0**	**35.5**	**37.2**	**35.7**	**33.5**	**33.6**	**33.6**	**34.5**	**34.2**	**43.8**	**19.6**
Rare earth elements (ppm)											
La	19.0	10.3	12.6	14.0	4.11	6.67	4.58	4.29	5.42	24.1	1.16
Ce	38.1	24.4	30.7	31.1	9.83	15.2	10.9	9.82	12.5	58.5	4.17
Pr	5.46	3.45	4.06	4.32	1.48	2.26	1.59	1.48	1.87	7.41	0.905
Nd	26.2	16.8	18.4	20.5	7.21	10.8	7.82	7.16	9.06	33.3	6.54
Sm	7.37	4.66	4.75	5.59	2.25	3.15	2.52	2.28	2.68	7.79	3.61
Eu	2.46	1.57	1.63	1.89	0.867	1.14	0.914	0.843	0.884	2.73	1.35
Gd	7.76	4.98	5.24	5.99	3.30	4.24	3.21	3.17	3.02	7.95	3.83
Tb	1.06	0.699	0.797	0.852	0.638	0.797	0.573	0.594	0.465	1.12	0.315
Dy	6.53	4.37	5.92	5.61	4.30	5.33	3.76	3.94	2.77	6.50	1.06
Ho	1.16	0.852	1.23	1.08	0.919	1.13	0.783	0.818	0.555	1.21	0.156
Er	2.94	2.36	3.33	2.88	2.52	3.11	2.12	2.20	1.44	3.25	0.359
Tm	0.374	0.329	0.509	0.404	0.373	0.456	0.303	0.317	0.205	0.453	0.044
Yb	2.30	2.32	3.29	2.64	2.44	2.95	1.87	2.00	1.32	2.98	0.263
Lu	0.297	0.316	0.453	0.355	0.363	0.436	0.258	0.282	0.192	0.456	0.036
Y	32.8	24.3	35.0	30.7	28.4	35.0	23.9	25.0	16.6	31.2	4.74

* Note that TiO_2 and K_2O are major elements of some samples, but are shown as trace elements for consistency.
** In wt%.

the raw counts. The Fe^{2+}/Fe^{3+} ratios of garnet and omphacite were calculated by charge balance. The *in situ* trace element contents of minerals were measured at the Institute of Mineralogy, Universität Würzburg using a LA-ICP-MS (Agilent 7500i, NewWave LUV 266×) (see above). The ablation patterns were single spots (40 μm) with a repetition rate of 5 Hz. For silicates, a laser energy of 0.40 to 0.56 mJ and a laser density of ~44 J/cm^2; for carbonates and phosphates, the laser energy was reduced to 0.13 to 0.3 mJ and a laser density of ~10 J/cm^2 resulting in smaller spots (30 μm). For the apatite and ankerite measurements the Ca-content of the respective minerals—obtained by the electron microprobe—was used as internal standard. For silicates and titanite Si was used as internal standard and Ti for rutile. In order to check the analytical accuracy, analyses of minor elements in all minerals were compared to the respective microprobe results and, in addition, synthetic rutile and titanite (courtesy of T. Zack, 2005) were analyzed and used for the comparison of trace elements. The calculation of trace element concentrations was conducted by the GLITTER Version 3.0 on-line interactive data reduction for LA-ICP-MS Program by Macquarie Res. (2000). The 1σ error based on counting statistics from signal and background is <10%. The mean detection limits (DL) for all runs (3-sigma) are for silicates, carbonates and rutile: K = 6, 11, 9 ppm; Rb = 0.17, 0.31, 0.24 ppm; Sr = 0.07; 0.14, 0.09 ppm; Ba = 0.49, 0.92, 0.57 ppm; Pb = 0.27, 0.55, 0.44 ppm; Ti = 19, 26, - ppm; Nb = 0.07, 0.13, 0.09 ppm; Ta = 0.05, 0.12, 0.06 ppm; Zr = 0.13, 0.27, 0.18 ppm; Hf = 0.16, 0.39; 0.22 ppm; P = 62, 102, 65 ppm; La = 0.05, 0.11, 0.08 ppm; Ce = 0.05, 0.11, 0.08 ppm; Nd = 0.25, 0.58, 0.35 ppm; Sm = 0.30, 0.70, 0.44 ppm; Eu = 0.08, 0.17, 0.12 ppm; Yb = 0.23, 0.55, 0.28 ppm; Y = 0.06, 0.13, 0.09 ppm; Th = 0.07, 0.17, 0.10 ppm; and U = 0.05, 0.11, 0.08 ppm, respectively. However, if the DL of some individual measurements are lower than the mean DL the measured values are shown in Table 4. The mineral abbreviations used in this paper are after Kretz (1983), except: Omp = omphacite, Amp = amphibole, Ph = phengite.

5. RESULTS

5.1. Fluid inclusion study

Primary, tubular, two-phase, aqueous fluid inclusions were entrapped in the fibrous omphacite and in omphacite inclusions in garnet of the segregation (Fig. 4a and b), as well as in matrix omphacite of the host eclogite (Sample TS33-5B; Fig. 4c). Fluid inclusions with a length of 5–15 μm usually occur as isolated tubes with their long dimension parallel to the *c*-axes of the host omphacite. The liquid/vapor ratios of inclusions are more or less constant with filling degrees of 85–90 vol%, suggesting that"necking down" or partial decrepitation after entrapment did not occur. The freezing temperature between −32.9 and −36.4 °C is characterized by the sudden shrinkage of the vapor bubble with initial melting > − 32.9 °C, indicating a predominantly NaCl–KCl–H_2O system (cf. Klemd, 1989). The final melting temperature (Tmf) varies from −0.9 to −2.7 (Fig. 5a) displaying low salinities of 1.57 to 4.49 wt% NaCl equivalent for these inclusions, similar to those reported for primary inclusions in omphacite in eclogites from the same area (cf. Gao and Klemd, 2001). The homogenization temperature (Th) varies between 175 and 240 °C (Fig. 5b). Calculated densities range between 0.81 and 0.90 g/cm^3, using the program of Bakker (2003).

Tubular two- to three-phase aqueous fluid inclusions with a length of 8–20 μm have their long dimension parallel to the *c*-axes of the host omphacite. A liquid, a gas bubble ± a solid

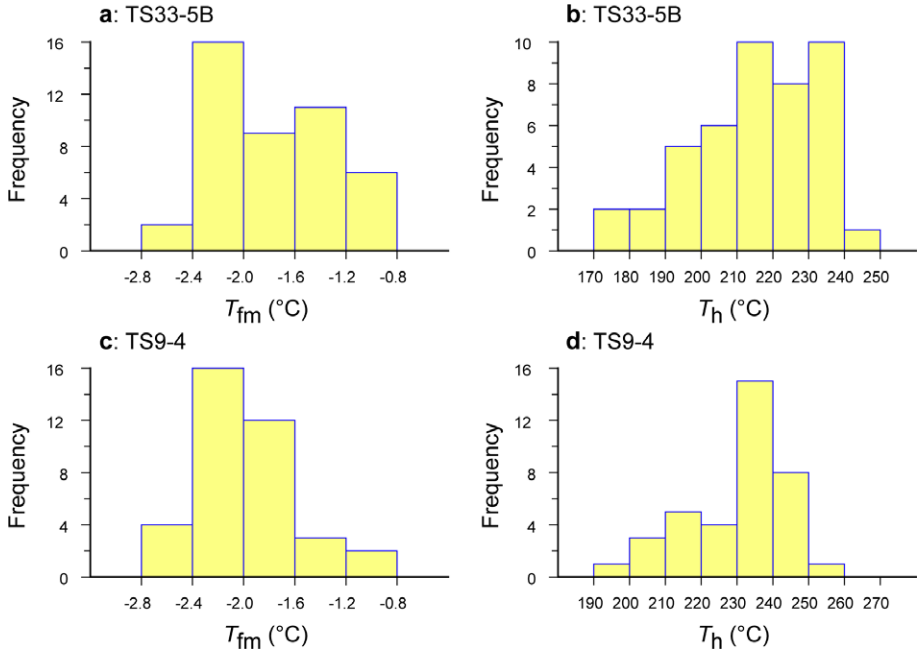

Fig. 5. Histograms showing final melting temperatures (a and c) and homogenization temperatures (b and d) for primary fluid inclusions in omphacites from the segregation (sample TS33-5B), the vein (sample TS9-4) and their host eclogites.

inclusion were observed in both the core and the rim of the fibrous vein and host omphacite of sample TS9-4 (Fig. 4d and e). The solid inclusion, which constitutes less than 10% of the fluid inclusion volume, has been identified as calcite and siderite by laser Raman spectroscopy (Fig. 4f). These carbonates may be due to back-reactions between the omphacite host and a low-salinity, aqueous fluid with minor CO_2 (e.g., Heinrich and Gottschalk, 1995; Franz et al., 2001) or are accidentally trapped. However, the gas bubble and the liquid does not contain any significant amount of CO_2 (>1 mol%) as revealed by Raman spectroscopy, which was already indicated by the absence of clathrate melting. The freezing temperature of inclusions varies from −34.0 and −37.4 °C with initial melting > − 34 °C, and Tmf varies from −1.5 to −2.7 °C (Fig. 5c), also indicating low salinities of 2.57 to 4.49 wt% NaCl equivalent in a NaCl–KCl–H_2O dominant system (cf. Klemd, 1989) for these inclusions in the fibrous omphacite of the vein. Th varies from 192 to 259 °C (Fig. 5d). Calculated densities range between 0.80 and 0.89 g/cm^3 almost identical to those ones from the segregation.

In both samples homogenization temperatures vary with almost constant final melting temperatures indicating re-equilibration by the stretching of a single fluid inclusion population during which the densities of the fluid inclusions decreased (cf. Goldstein and Reynold, 1994).

5.2. Major and trace element compositions of host eclogites

5.2.1. Host rock of the segregation, locality 1

Three whole-rock samples TS33-5A, TS33-5B, and TS33-2 provide a representative estimate of the composition of the host eclogite away from the segregation (Fig. 2i; Tables 1 and 2), The average host eclogite has a basaltic composition with $SiO_2 = 55.12$ wt%, $Na_2O = 5.68$ wt%, and $TiO_2 = 0.8$ wt%. The average loss of ignition (LOI) is 1.65 wt%. The chondrite-normalized REE pattern indicate an enriched mantle source from which the precursor melt was generated (Fig. 6a), with a total LREE concentration of 60 to 40 times chondrite, a $(La/Sm)_N$ value of 1.56, and a $(La/Yb)_N$ value of 2.7. The MORB-normalized trace element patterns show a scattered distribution (Fig. 5b); both LILE (Cs, Rb, Ba, K, Pb, and Sr) and the HFSE and P display pronounced negative anomalies compared with rare earth elements (Fig. 6b). The fluid mobile LILE are typically erratic in eclogites (e.g., John et al., 2004), and are thus shown separately in the figure. However, HFSE are usually rather unaffected by metamorphic processes and are thus frequently used to determine the genesis of the precursor rock prior to metamorphism. Nb/Ta ratios lie between 13 and 14 and Zr/Hf between 35 and 37 and are typical for oceanic basalts (e.g., Pfänder et al., 2007).

A profile comprising five samples of host eclogite taken at various distances to the segregation was conducted. The sample localities are shown in Fig. 2k. Each sample is 1×2 cm^2 in plain view and 0.5 cm thick. According to their distance to the segregation they are named TS33-5B-a = (a) which is 7.3 cm away, (b) = 5.7 cm; (c) = 3.7 cm; (d) = 2.8 cm; (e) = 1.5 cm away from the segregation. The variations in the major elements might be somewhat ambiguous due to the small sample size in comparison to the grain size. However, some patterns are still evident; Al_2O_3 contents continuously decrease towards the segregation, whereas MgO, CaO, and Na_2O display a continuous increase. The most prominent feature along this profile is the continuous decrease in concentration of some of the HFSE (Ti, Nb, and Ta), the LILE (K, Rb, Ba, Sr, and Pb) and the HREE + Y as well as the relative increase of Zr, Hf, and P towards the segregation (Fig. 7a and b). Most of these trace elements occur in minerals with a small grain size and a homogenous distribution in the rock. The distribution of zircon grains for example was checked by BSE-imaging. The U, Th, and LREE contents remain almost constant across the profile. Both Nb/Ta and Zr/Hf ratios are relatively constant (13 to 15 and around 34) and display no systematic variations.

5.2.2. Host rock of the vein, locality 2

The eclogite host of the vein has the following composition in wt% $SiO_2 = 38.2$, $Al_2O_3 = 15.3$, $Na_2O = 3.62$, $K_2O = 0.99$, $TiO_2 = 4.39$, and $CaO = 12.73$. This composition

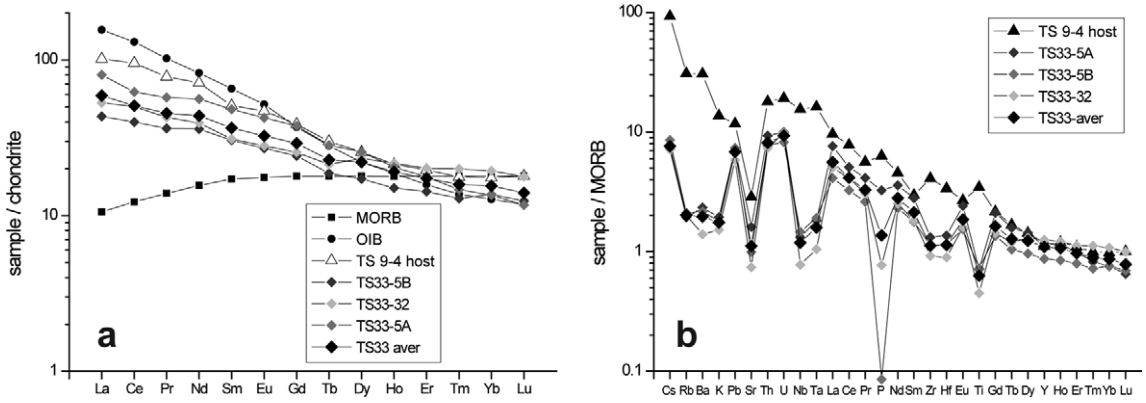

Fig. 6. Chondrite-normalized rare earth element pattern (a) and MORB-normalized trace element pattern (b) of the host eclogites from the western Tianshan high-pressure low-temperature metamorphic belt in northwestern China. Normalization-values are taken from Sun and McDonough (1989).

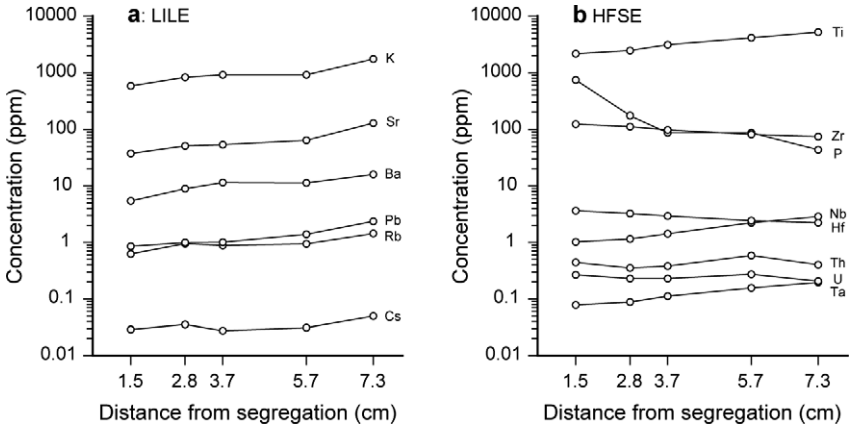

Fig. 7. Chemical composition of the segregation host eclogite along a profile with variable distance to the segregation. (a) LILE and (b) HFSE.

indicates that the basaltic protolith underwent spilitization. The high loss of ignition (6.58 wt%) and the CaO content (12.73 wt%) is in accordance with large modal amounts of calcite and ankerite in the rocks, suggesting an extensive hydrothermal seafloor alteration prior to metamorphism. The chondrite-normalized REE pattern of this host eclogite shows LREE enrichment and a flat-HREE distribution (Fig. 6a), with large amounts of LREE (100 to 50 times chondritic), a $(La/Sm)_N$ value of about 2 and a $(La/Yb)_N$ value of ~5.5, all of which are typical of melts generated in an enriched mantle source. MORB-normalized trace element patterns display a steep negative slope and are rather similar to that of a typical ocean-island-basalt, suggesting a seamount scenario in which the precursor rock may have formed (Fig. 6b). Nb/Ta ratios are ~17 and Zr/Hf ~44, and are thus within the accepted range for oceanic basalts (e.g., Pfänder et al., 2007).

5.3. Chemical composition of minerals

Major element compositions of the representative minerals are presented in Table 3. Average contents of LILE (K, Rb, Ba, Pb, and Sr), HFSE (Ti, Nb, Ta, Zr, and Hf), REE (La, Ce, Nd, Sm, Eu, and Yb) and Y of the representative minerals are presented in Table 4.

5.3.1. Garnet

Idioblastic garnet 1 from the segregation is almost unzoned in major elements and displays a composition of ~$Alm_{64}Prp_{13}Grs_{21}Sps_2$ (Table 3). The trace elements show no zoning, with the exception of Y and Yb, which show a relative enrichment (108 and 10.4 ppm for core and 317 and 28.1 ppm for rim, respectively) and a depletion of all other REE, LILE, and HFSE (frequently below detection limits). However, garnet 2 in the segregation host eclogite shows well-defined major-element prograde growth zoning, indicated by an increase of the pyrope/almandine ratio and a decrease of the spessartine component. Garnet 2 has a core composition of $Alm_{67}Prp_9Grs_{21}Sps_3$ and a rim composition of $Alm_{68}Prp_{13}Grs_{18}Sps_1$ (Table 3). All trace elements, including Y and Yb (136 and 11.1 ppm for cores) are rather similar in concentrations in the cores and rims. The Ti and Zr concentrations slightly decrease from the core to the rim (e.g., Ti decreases from 608 to 449 ppm).

Idioblastic garnet in the eclogite host to the vein shows a very small prograde growth zoning in its major elements, with a core of ~$Alm_{69}Prp_5Grs_{23}Sps_3$ and a rim of ~$Alm_{68}Prp_8Grs_{23}Sps_1$. It is, however, zoned with respect to trace elements. Concentration of Ti and REE decrease from core to rim (where it is frequently below detection limit). Ti drops from 943 to 472 ppm and Y and Yb from 226 and 18.1 ppm to 104 and 10.7 ppm, respectively (Table 4).

5.3.2. Omphacite

The jadeite component of fibrous omphacite (average 50 mol%) from the segregation is similar to that of the rim of matrix omphacite (average 52 mol%) from the host eclogite. The jadeite component of the omphacite inclusion in garnet (48 mol%) in the segregation is slightly higher than that of the core of matrix omphacite (42 mol%) in the host eclogite. The matrix omphacite from the eclogite host of the segregation shows compositional zoning defined by an increasing jadeite component (e.g., from 41 to 58 mol%) and a decreasing aegirine component (e.g., from 22.4 to 0 mol%) from core to rim (Table 3). Omphacite from the eclogite host of the segregation contains more trace elements in the grain core than in the grain rim (Table 4); in average omphacite contains 409 ppm Ti, 202 ppm K, 38.9 ppm P, 3.36 ppm Rb, 3.80 ppm Y. Pb and REE are below 1 ppm in their concentrations.

Fibrous omphacite from the vein generally contains dark irregular cores that are rimmed by lighter-colored pyroxene (Fig. 3e). The core ($X_{Jd} = 44.5$) and rim ($X_{Jd} = 46$) display similar jadeite contents, which both resemble that of omphacite inclusions in the garnet from the host eclogite ($X_{Jd} = 46$). All these values, however, are greater than that of matrix omphacite ($X_{Jd} = 39$). The core of omphacite from the vein contains a higher trace element concentration than the rim (average compositions e.g., 604 ppm vs. 18.5 ppm K, 1.32 ppm vs. 0.252 ppm Rb, 12.1 ppm vs. 0.726 ppm Ba). Matrix omphacite from the

Table 3
Representative major element composition of minerals in the eclogite facies segregation, vein and their host eclogites

Sample:	TS33-5B	TS33-5B	TS33-5B	TS33-5B	TS9-4	TS9-4	TS33-5B	TS33-5B	TS33-5B	TS33-5B	TS9-4	TS9-4	TS9-4	TS9-4	TS9-4	TS33-5B	TS33-5B	TS33-5B	TS33-5B	TS9-4	TS9-4	TS9-4	TS9-4
Location:	Segregation	Segregation	Host	Host	Host	Host	Segregation	Segregation	Host	Host	Vein	Vein	Vein	Host	Host	Segregation	Segregation	Host	Host	Vein	Host	Host	Host
Mineral	Grt-C	Grt-R	Grt-C	Grt-R	Grt-C	Grt-R	Omp-I	Omp	Omp-C	Omp-R	Omp-C	Omp-R	Ab-I	Omp-I	Omp	Pg	Ph	Pg-I	Pg	Ph	Pg-I	Pg	Ph
SiO_2	38.32	38.63	38.42	38.88	38.27	38.26	56.83	56.46	56.52	57.92	55.64	56.61	69.38	55.81	55.53	48.76	51.44	48.96	47.68	50.34	48.34	49.44	49.23
TiO_2	0.04	0.02	0.07	0.05	0.24	0.00	0.00	0.05	0.04	0.04	0.00	0.05	0.00	0.09	0.08	0.13	0.37	0.05	0.02	0.45	0.01	0.06	0.35
Al_2O_3	21.30	21.65	21.56	21.65	21.48	21.41	11.14	11.63	10.46	12.67	11.03	10.86	19.40	9.52	8.86	38.77	28.05	38.52	38.10	28.43	40.67	39.08	27.92
Cr_2O_3	0.01	0.03	0.00	0.01	0.00	0.02	0.03	0.00	0.01	0.00	0.02	0.02	0.03	0.01	0.00	0.07	0.01	0.01	0.00	0.07	0.02	0.00	0.01
FeO	28.94	30.17	29.72	27.47	29.54	29.84	6.96	7.40	8.89	3.94	8.14	7.35	0.15	10.92	10.72	0.28	2.34	0.62	0.27	3.54	0.21	0.33	3.44
Fe_2O_3	n.c.	n.c.	n.c.	n.c.	n.c.	n.c.	n.c.	n.c.	n.c.	n.c.	n.c.	n.c.	n.c.	n.c.	n.c.	n.c.	n.c.	n.c.	n.c.	n.c.	n.c.	n.c.	n.c.
NiO	0.07	0.00	0.00	0.00	0.00	0.01	0.00	0.00	0.07	0.00	0.05	0.04	0.00	0.00	0.02	0.00	0.00	0.01	0.04	0.04	0.00	0.00	n.d.
MnO	1.49	0.55	0.65	0.33	1.07	0.41	0.05	0.11	0.06	0.04	0.00	0.00	0.00	0.02	0.03	0.00	0.00	0.00	0.05	0.04	0.05	0.05	0.00
MgO	2.14	3.19	3.24	3.40	1.22	1.92	6.03	6.00	5.42	6.92	5.60	5.34	0.01	4.87	5.05	0.18	2.82	0.25	0.21	2.54	0.08	0.15	2.84
CaO	7.19	6.34	6.53	8.26	7.79	7.86	10.72	10.79	10.06	11.51	10.81	10.27	0.36	9.89	9.98	0.17	0.00	0.13	0.15	0.00	0.82	0.16	0.01
Na_2O	0.05	0.00	0.04	0.08	0.00	0.04	8.67	7.76	9.13	8.30	7.95	8.45	10.97	8.96	8.58	5.96	0.81	6.44	6.00	0.75	6.10	6.29	0.88
K_2O	0.01	0.00	0.01	0.00	0.00	0.00	0.00	0.01	0.00	0.01	0.01	0.01	0.03	0.01	0.01	1.14	9.71	1.18	0.87	9.05	0.25	0.45	9.91
P_2O_5	n.d.	n.d.	n.d.	n.d.	n.d.	n.d.	n.d.	n.d.	n.d.	n.d.	n.d.	n.d.	n.d.	n.d.	n.d.	n.d.	n.d.	n.d.	n.d.	n.d.	n.d.	n.d.	n.d.
F	n.d.	n.d.	n.d.	n.d.	n.d.	n.d.	n.d.	n.d.	n.d.	n.d.	n.d.	n.d.	n.d.	n.d.	n.d.	n.d.	n.d.	n.d.	n.d.	n.d.	n.d.	n.d.	n.d.
CL	n.d.	n.d.	n.d.	n.d.	n.d.	n.d.	n.d.	n.d.	n.d.	n.d.	n.d.	n.d.	n.d.	n.d.	n.d.	n.d.	n.d.	n.d.	n.d.	n.d.	n.d.	n.d.	n.d.
H_2O	n.c.	n.c.	n.c.	n.c.	n.c.	n.c.	n.c.	n.c.	n.c.	n.c.	n.c.	n.c.	n.c.	n.c.	n.c.	4.73	4.53	4.75	4.63	4.50	4.80	4.77	4.44
Total	99.56	100.58	100.24	100.13	99.61	99.77	100.43	100.21	100.66	101.35	99.25	99.00	100.33	100.10	98.86	100.19	100.08	100.92	98.02	99.75	101.35	100.78	99.03
Si	3.07	3.05	3.04	3.06	3.08	3.06	2.01	2.02	2.00	2.02	2.01	2.04	3.01	2.00	2.02	3.09	3.41	3.09	3.09	3.36	3.02	3.11	3.32
Al	2.01	2.01	2.01	2.01	2.03	2.01	0.46	0.49	0.44	0.52	0.47	0.46	0.99	0.40	0.38	2.89	2.19	2.87	2.91	2.23	3.00	2.89	2.22
Cr	0.00	0.00	0.00	0.00	0.00	0.00	0.00	0.00	0.00	0.00	0.00	0.00	0.00	0.00	0.00	0.00	0.00	0.00	0.00	0.00	0.00	0.00	0.00
Ti	0.00	0.00	0.00	0.00	0.02	0.00	0.00	0.00	0.00	0.00	0.00	0.00	0.00	0.00	0.00	0.01	0.02	0.00	0.00	0.02	0.00	0.00	0.02
Fe^3+	0.00	0.00	0.00	0.00	0.00	0.00	0.11	0.01	0.19	0.01	0.07	0.05	0.00	0.21	0.18	0.00	0.00	0.00	0.00	0.00	0.00	0.00	0.00
Fe^2+	1.94	1.99	1.97	1.81	1.99	1.99	0.10	0.21	0.08	0.11	0.18	0.18	0.01	0.12	0.15	0.02	0.13	0.03	0.02	0.20	0.01	0.02	0.19
Ni	0.00	0.00	0.00	0.00	0.00	0.00	0.00	0.00	0.00	0.00	0.00	0.00	0.00	0.00	0.00	0.00	0.00	0.00	0.00	0.00	0.00	0.00	0.00
Mn	0.10	0.04	0.04	0.02	0.07	0.03	0.00	0.00	0.00	0.00	0.00	0.00	0.00	0.00	0.00	0.00	0.00	0.00	0.00	0.00	0.00	0.00	0.00
Mg	0.26	0.38	0.38	0.40	0.15	0.23	0.32	0.32	0.29	0.36	0.30	0.29	0.00	0.26	0.27	0.02	0.28	0.02	0.02	0.25	0.01	0.01	0.29
Ca	0.62	0.54	0.55	0.70	0.67	0.67	0.41	0.41	0.38	0.43	0.42	0.40	0.02	0.38	0.39	0.01	0.00	0.01	0.01	0.00	0.06	0.01	0.00
Na	0.01	0.00	0.01	0.01	0.00	0.01	0.59	0.54	0.63	0.56	0.56	0.59	0.92	0.62	0.61	0.73	0.10	0.79	0.75	0.10	0.74	0.77	0.11
K	0.00	0.00	0.00	0.00	0.00	0.00	0.00	0.00	0.00	0.00	0.00	0.00	0.00	0.00	0.00	0.09	0.82	0.10	0.07	0.77	0.02	0.04	0.85
P	n.c.	n.c.	n.c.	n.c.	n.c.	n.c.	n.c.	n.c.	n.c.	n.c.	n.c.	n.c.	n.c.	n.c.	n.c.	n.c.	n.c.	n.c.	n.c.	n.c.	n.c.	n.c.	n.c.
F	n.c.	n.c.	n.c.	n.c.	n.c.	n.c.	n.c.	n.c.	n.c.	n.c.	n.c.	n.c.	n.c.	n.c.	n.c.	n.c.	n.c.	n.c.	n.c.	n.c.	n.c.	n.c.	n.c.
Cl	n.c.	n.c.	n.c.	n.c.	n.c.	n.c.	n.c.	n.c.	n.c.	n.c.	n.c.	n.c.	n.c.	n.c.	n.c.	n.c.	n.c.	n.c.	n.c.	n.c.	n.c.	n.c.	n.c.
Cation	8.01	8.01	8.00	8.01	8.01	8.00	4.00	4.00	4.01	4.01	4.01	4.01	4.95	3.99	4.00	6.86	6.95	6.91	6.87	6.93	6.86	6.85	7.00
O	12	12	12	12	12	12	6	6	6	6	6	6	8	6	6	12	12	12	12	12	12	12	12
XFe	0.66	0.67	0.67	0.62	0.69	0.68	0.12	0.22	0.11	0.12	0.20	0.21		0.16	0.19	0.40	0.32	0.50	0.40	0.44	0.13	0.50	0.40
WEF Alm	66.57	67.74	66.76	61.80	69.05	68.21	40.88	46.75	37.37	44.48	44.56	42.13		37.83	40.13								
JD And	0.00	0.00	0.00	0.00	0.00	0.00	47.85	51.86	43.99	54.81	48.19	52.71		40.82	40.72								
AE Grs	21.16	18.14	18.79	23.78	23.33	22.95	11.27	1.39	18.64	0.72	7.25	5.16		21.36	19.14								
Pyp	8.77	12.77	12.97	13.64	5.08	7.82																	
Sps	3.47	1.25	1.48	0.75	2.53	0.95																	

(*continued on next page*)

Table 3 (*continued*)

Sample:	TS33-5B	TS33-5B	TS9-4	TS9-4	TS9-4	TS33-5B	TS33-5B	TS9-4	TS33-5B	TS9-4	TS9-4	TS335-B	TS33-5B	TS9-4	TS9-4	TS33-5B	TS33-5B	TS9-4	TS9-4	TS9-4	TS33-5B	TS9-4
Location:	Segre-gation	Host	Vein	Vein	Host	Host	Host	Host	Segre-gation	Vein	Host	Segre-gation	Host	Vein	Vein	Segre-gation	Host	Vein	Vein	Host	Host	Host
Mineral	Gln	Gln	Gln	Bar	Cro-I	Zo-I	Zo	Zo-I	Ank	Ank	Ank	Ap	Ap	Ap	Ap	Rt	Rt	Rt-C	Rt-R	Rt	Ttn	Ttn
SiO_2	56.80	55.86	54.65	51.83	50.69	39.32	39.29	39.14	0.00	0.00	0.00	n.d.	n.d.	n.d.	n.d.	0.02	0.03	0.06	0.05	0.03	30.38	31.08
TiO_2	0.07	0.12	0.10	0.16	0.13	0.30	0.02	0.08	0.00	0.03	0.00	n.d.	n.d.	n.d.	n.d.	98.68	98.53	98.21	98.34	98.38	37.52	37.19
Al_2O_3	10.77	11.80	11.48	6.95	10.54	29.56	27.94	28.76	0.03	0.02	0.00	n.d.	n.d.	n.d.	n.d.	0.01	0.01	0.00	0.00	0.01	1.86	2.13
Cr_2O_3	0.04	0.02	0.05	0.03	0.00	0.00	0.00	0.03	0.00	0.04	0.00	n.d.	n.d.	n.d.	n.d.	0.00	0.02	0.05	0.02	0.04	0.10	0.00
FeO	12.03	11.98	14.81	13.92	14.52	n.d.	n.d.	n.d.	9.83	10.69	12.17	0.76	0.00	0.00	1.15	0.50	0.80	1.17	1.40	0.32	0.27	0.19
Fe_2O_3	n.c.	n.c.	n.c.	n.c.	n.c.	4.32	6.34	4.96	n.c.	n.c.	n.c.	n.c.	n.c.	n.c.	n.c.	n.c.	n.c.	n.c.	n.c.	n.c.	n.c.	n.c.
NiO	0.00	0.00	0.05	0.00	0.05	0.03	0.05	0.06	0.03	0.00	0.06	n.d.	n.d.	n.d.	n.d.	0.00	0.00	0.03	0.00	0.04	0.02	0.00
MnO	0.00	0.05	0.03	0.02	0.06	0.04	0.00	0.08	0.03	0.15	0.24	0.00	0.06	0.20	0.17	0.05	0.05	0.00	0.00	0.00	0.06	0.00
MgO	8.92	8.75	7.87	12.55	4.50	0.12	0.04	0.08	16.82	14.99	13.31	0.03	0.04	0.00	0.02	0.00	0.02	0.02	0.00	0.00	0.00	0.00
CaO	1.07	1.52	1.80	7.58	8.52	23.52	23.67	23.08	28.72	27.85	27.18	53.85	53.59	53.74	53.92	0.00	0.00	0.01	0.02	0.12	27.98	28.15
Na_2O	6.99	6.91	6.43	4.21	7.26	0.00	0.00	0.04	0.01	0.05	0.06	n.d.	n.d.	n.d.	n.d.	0.03	0.02	0.00	0.00	0.25	0.03	0.05
K_2O	0.00	0.06	0.08	0.21	0.14	0.00	0.00	0.01	0.00	0.01	0.00	n.d.	n.d.	n.d.	n.d.	0.00	0.01	0.00	0.01	0.05	0.00	0.00
P_2O_5	n.d.	n.d.	n.d.	n.d.	n.d.	n.d.	n.d.	n.d.	n.d.	n.d.	n.d.	42.93	43.46	42.84	42.33	n.d.	n.d.	n.d.	n.d.	n.d.	n.d.	n.d.
F	n.d.	n.d.	n.d.	n.d.	n.d.	n.d.	n.d.	n.d.	n.d.	n.d.	n.d.	2.08	2.12	2.55	2.35	n.d.	n.d.	n.d.	n.d.	n.d.	n.d.	n.d.
Cl	n.d.	n.d.	n.d.	n.d.	n.d.	n.d.	n.d.	n.d.	n.d.	n.d.	n.d.	0.00	0.01	0.00	0.01	n.d.	n.d.	n.d.	n.d.	n.d.	n.d.	n.d.
H_2O	n.c.	n.c.	n.c.	n.c.	n.c.	n.c.	n.c.	n.c.	n.c.	n.c.	n.c.	n.c.	n.c.	n.c.	n.c.	n.c.	n.c.	n.c.	n.c.	n.c.	n.c.	n.c.
Total	96.69	97.07	97.35	97.46	96.41	97.21	97.35	96.32	55.47	53.83	53.02	99.65	99.28	99.33	99.95	99.29	99.49	99.55	99.84	99.24	98.22	98.79
Si	7.95	7.81	7.69	7.44	7.22	3.04	3.06	3.06	0.00	0.00	0.00	n.c.	n.c.	n.c.	n.c.	0.00	0.00	0.00	0.00	0.00	1.01	1.02
Al	1.77	1.94	1.90	1.18	1.77	2.69	2.56	2.65	0.00	0.00	0.00	n.c.	n.c.	n.c.	n.c.	0.00	0.00	0.00	0.00	0.00	0.07	0.08
Cr	0.00	0.00	0.01	0.00	0.00	0.00	0.00	0.00	0.00	0.00	0.00	n.c.	n.c.	n.c.	n.c.	0.00	0.00	0.00	0.00	0.00	0.00	0.00
Ti	0.01	0.01	0.01	0.02	0.01	0.02	0.00	0.01	0.00	0.00	0.00	n.c.	n.c.	n.c.	n.c.	0.99	0.99	0.99	0.98	0.99	0.94	0.92
Fe^3+	0.10	0.07	0.39	0.36	1.73	0.25	0.37	0.29	0.26	0.29	0.34	n.c.	n.c.	n.c.	n.c.	0.00	0.00	0.00	0.00	0.00	0.00	0.00
Fe^2+	1.31	1.33	1.35	1.31	0.00	0.00	0.00	0.00	n.c.	n.c.	n.c.	0.05	0.00	0.00	0.08	0.01	0.01	0.01	0.02	0.00	0.01	0.01
Ni	0.00	0.00	0.00	0.00	0.00	0.00	0.00	0.00	0.00	0.00	0.00	n.c.	n.c.	n.c.	n.c.	0.00	0.00	0.00	0.00	0.00	0.00	0.00
Mn	0.00	0.01	0.00	0.00	0.01	0.00	0.00	0.01	0.00	0.00	0.01	0.00	0.00	0.01	0.01	0.00	0.00	0.00	0.00	0.00	0.00	0.00
Mg	1.86	1.82	1.65	2.69	0.96	0.01	0.01	0.01	0.78	0.73	0.67	0.00	0.01	0.00	0.00	0.00	0.00	0.00	0.00	0.00	0.00	0.00
Ca	0.16	0.23	0.27	1.17	1.30	1.95	1.97	1.93	0.96	0.97	0.98	4.64	4.61	4.66	4.67	0.00	0.00	0.00	0.00	0.00	0.99	0.99
Na	1.90	1.87	1.75	1.17	2.01	0.00	0.00	0.01	0.00	0.00	0.00	n.c.	n.c.	n.c.	n.c.	0.00	0.00	0.00	0.00	0.01	0.00	0.00
K	0.00	0.01	0.01	0.04	0.03	0.00	0.00	0.00	0.00	0.00	0.00	n.c.	n.c.	n.c.	n.c.	0.00	0.00	0.00	0.00	0.00	0.00	0.00
P	n.c.	n.c.	n.c.	n.c.	n.c.	n.c.	n.c.	n.c.	n.c.	n.c.	n.c.	2.92	2.95	2.93	2.90	n.c.	n.c.	n.c.	n.c.	n.c.	n.c.	n.c.
F	n.c.	n.c.	n.c.	n.c.	n.c.	n.c.	n.c.	n.c.	n.c.	n.c.	n.c.	1.06	1.08	1.30	1.21	n.c.	n.c.	n.c.	n.c.	n.c.	n.c.	n.c.
Cl	n.c.	n.c.	n.c.	n.c.	n.c.	n.c.	n.c.	n.c.	n.c.	n.c.	n.c.	0.00	0.00	0.00	0.00	n.c.	n.c.	n.c.	n.c.	n.c.	n.c.	n.c.
Cation	15.06	15.10	15.03	15.38	15.04	7.96	7.97	7.97	2.00	1.99	2.00	8.67	8.65	8.91	8.86	1.00	1.00	1.00	1.00	1.00	3.02	3.02
O	23	23	23	23	23	12.5	12.5	12.5				12	12	12	12	2	2	2	2	2	5	5
XFe	0.39	0.39	0.41	0.25	0.00				0.13	0.15	0.17											

(i) WEF, diopside + hedenbergite; JD, jadeite; AE, aegirine; Alm, almandine; And, andradite; Grs, grossular; Pyp, pyrope; Sps, spessartine. (ii) C, the core of mineral; R, the rim of mineral; l, inclusion mineral. (iii) n.c, not calculated; n.d., not determined; H_2O was calculated assuming stoichiometric mineral compositions.

Table 4
Average trace element data of rock forming and accessory minerals of the segregation, the vein and their host eclogites

Sample	TS9-4	TS9-4	TS33-5B	TS33-5B	TS33-5B	TS33-5B	TS33-5B	TS33-5B	TS33-5B	TS9-4	TS9-4	TS9-4	TS9-4	TS33-5B
Mineral	Garnet	Garnet	Garnet	Garnet	Garnet	Garnet	Garnet	Garnet	Garnet	Omphacite	Omphacite	Omphacite	Omphacite	Omphacite
Position	core	rim	core	rim	core	rim	rim	rim	rim			core	rim	core
Location	Host of vein	Host of vein	Host of segr.	Host of segr.	Segregation	Segregation	Host (58 mm to seg.)	Host (40 mm to seg.)	Host (1 mm to the seg.)	Host of vein	Vein	Vein	Vein	Host of segr.
n	2	2	2	2	2	5	1	1	1	4	4	11	11	1
K	nd	nd	nd	nd	nd	nd	nd	nd	nd	168	49.1	604	18.5	26.6
Rb	nd	nd	nd	nd	nd	nd	nd	nd	nd	0.500	*0.202*	1.32	0.252	2.11
Sr	nd	nd	nd	nd	nd	nd	nd	nd	nd	22.6	26.7	34.2	21.8	11.3
Ba	nd	nd	nd	nd	nd	nd	nd	nd	nd	2.80	1.25	12.1	0.726	5.67
Pb	bdl	bdl	bdl	bdl	bdl	bdl	0.481	bdl	0.526	0.456	0.481	0.536	0.298	bdl
Ti	943	472	712	349	608	449	1432	792	464	627	640	534	517	1728
Nb	bdl	bdl	bdl	bdl	bdl	bdl	1.15	0.590	bdl	0.369	0.079	0.071	*0.066*	0.642
Ta	bdl	bdl	bdl	bdl	bdl	bdl	bdl	0.089	bdl	bdl	bdl	bdl	bdl	bdl
Zr	1.30	1.95	8.75	*1.68*	2.12	1.78	2.80	5.28	1.51	0.90	0.799	1.47	0.831	3.94
Hf	0.141	0.669	bdl	bdl	bdl	bdl	bdl	bdl	bdl	0.194	0.120	0.124	0.139	bdl
P	nd	nd	nd	nd	nd	nd	nd	nd	nd	bdl	35.5	*30.0*	*40.9*	bdl
La	13.2	bdl	1.90	1.46	*0.10*	*0.092*	0.241	0.097	bdl	0.117	*0.113*	0.167	0.041	0.074
Ce	49.1	bdl	4.94	*3.96*	bdl	bdl	bdl	0.089	bdl	0.281	0.127	0.352	0.082	0.294
Nd	22.4	bdl	7.15	*2.93*	bdl	*0.554*	bdl	0.723	bdl	*0.331*	*0.401*	0.406	0.249	0.465
Sm	8.08	2.49	2.74	1.38	*1.06*	1.45	0.899	b.l.	1.54	*0.230*	*0.432*	0.286	0.286	0.261
Eu	3.84	1.12	1.54	1.05	0.662	1.02	0.799	1.09	1.21	*0.089*	0.130	0.177	0.125	0.182
Yb	18.1	10.7	10.4	28.1	11.1	11.0	17.0	13.8	9.51	0.243	bdl	0.135	bdl	0.667
Y	226	104	108	317	136	122	228	215	76.1	0.823	0.575	0.425	0.305	2.66
Th	bdl	bdl	bdl	bdl	bdl	bdl	bdl	bdl	bdl	bdl	bdl	bdl	bdl	bdl
U	bdl	bdl	bdl	bdl	bdl	bdl	bdl	bdl	bdl	bdl	bdl	bdl	bdl	0.035
Nb/Ta														
Zr/Hf														

Sample	TS33-5B	TS33-5B	TS33-5B	TS33-5B	TS33-5B	TS33-5B	TS33-5B	TS9-4	TS33-5B	TS9-4	TS9-4	TS33-5B	TS33-5B	TS9-4/33-5B
Mineral	Omphacite	Omphacite	Omphacite	Omphacite	Omphacite	Omphacite	Omphacite	Phengite	Phengite	Paragonite	Paragonite	Paragonite	Paragonite	Glaucophane
Position	rim			core	core	Core	core							
Location	Host of segr.	Host of segr.	Segregation	Host (58 mm to seg.)	Host (22 mm to seg.)	Host (12 mm to seg.)	Host (0 mm to seg.)	Vein	Segregation	Host of vein	Vein	Host of segr.	Segregation	
n	1	2	6	1	1	1	1	10	3	2	2	5	5	10
K	74.5	202	21.8	181	26.6	1323	9.25	74270	74353	6508	4972	4600	5418	561
Rb	0.252	0.960	*0.143*	1.50	bdl	2.11	bdl	205	249	3.12	5.32	2.66	6.87	0
Sr	7.89	13.0	11.5	14.8	6.14	16.5	12.6	100	49.6	417	4208	597	518	5.83
Ba	1.06	3.36	*0.400*	2.08	0.743	10.6	bdl	2014	1791	72.2	95.7	66.7	98.3	1.10
Pb	0.264	0.300	0.275	0.219	bdl	0.272	0.168	3.42	1.75	1.89	0.827	3.75	3.39	0.497
Ti	584	409	643	5705	2017	1438	538	nd	nd	nd	nd	nd	nd	928
Nb	0.114	bdl	0.037	3.73	0.469	0.815	0.058	nd	nd	nd	nd	nd	nd	0.115
Ta	bdl	bdl	bdl	0.169	bdl	0.052	bdl	nd	nd	nd	nd	nd	nd	bdl
Zr	0.793	0.875	0.963	11.1	0.669	7.21	0.978	nd	nd	nd	nd	nd	nd	1.31
Hf	0.091	0.221	0.161	0.286	bdl	0.298	0.175	nd	nd	nd	nd	nd	nd	0.107
P	28.5	39.0	*30.1*	31.2	bdl	bdl	bdl	nd	nd	nd	nd	nd	nd	32.2
La	0.022	0.046	*0.039*	0.053	0.115	0.033	bdl	0.042	bdl	0.074	0.018	0.121	0.156	bdl
Ce	0.060	0.100	0.074	0.167	0.508	0.079	bdl	0.088	0.071	bdl	0.127	0.157	0.116	0.154

(*continued on next page*)

Table 4 (*continued*)

Sample	TS33-5B	TS33-5B	TS33-5B	TS33-5B	TS33-5B	TS33-5B	TS33-5B	TS9-4	TS33-5B	TS9-4	TS9-4	TS33-5B	TS33-5B	TS9-4/33-5B
Mineral	Omphacite	Omphacite	Omphacite	Omphacite	Omphacite	Omphacite	Omphacite	Phengite	Phengite	Paragonite	Paragonite	Paragonite	Paragonite	Glaucophane
Position	rim			core	core	Core	core							
Location	Host of segr.	Host of segr.	Segregation	Host (58 mm to seg.)	Host (22 mm to seg.)	Host (12 mm to seg.)	Host (0 mm to seg.)	Vein	Segregation	Host of vein	Vein	Host of segr.	Segregation	
n	1	2	6	1	1	1	1	10	3	2	2	5	5	10
Nd	0.129	*0.261*	bdl	0.261	0.803	0.127	0.142	bdl	0.144	1.05	bdl	bdl	bdl	bdl
Sm	bdl	0.156	bdl	0.132	0.408	0.113	bdl	bdl	bdl	bdl	bdl	bdl	bdl	bdl
Eu	0.048	0.122	0.071	0.151	0.325	0.038	0.052	bdl	bdl	bdl	bdl	bdl	bdl	0.056
Yb	0.642	0.477	bdl	0.556	1.10	0.233	bdl	bdl	bdl	bdl	bdl	bdl	bdl	bdl
Y	1.59	3.80	0.667	5.05	4.37	0.957	0.332	bdl	0.079	0.465	0.080	0.269	bdl	0.359
Th	bdl	bdl	bdl	bdl	bdl	0.029	bdl	nd	nd	nd	nd	nd	nd	bdl
U	bdl	bdl	bdl	0.053	0.050	0.019	bdl	nd	nd	nd	nd	nd	nd	bdl
Nb/Ta														
Zr/Hf														

Sample	TS9-4/33-5E	TS9-4	TS33-5B	TS9-4/33-5E	TS9-4	TS33-5B	TS33-5B	TS33-5B	TS9-4	TS9-4	TS9-4	TS33-5B	TS33-5B
Mineral	Barrosite	Zoisite	Zoisite	Ankerite	Apatite	Apatite	Rutile	Rutile	Rutile	Rutile	Titanite	Titanite	Titanite
Position													
Location		Host of vein	Host of segr.		Vein	Host of segr.	Host of segr.	Segregation	Host of vein	Vein	Host of vein	Host of segr.	Segregation
n	6	4	5	8	7	1	3	13	1	11	4	4	4
K	1796	177	32.2	31.5	40.9	bdl	nd	nd	nd	nd	nd	nd	nd
Rb	0.679	0.630	0.122	0.747	0.145	0.357	nd	nd	nd	nd	nd	nd	nd
Sr	14.6	984	1775	1028	1940	587	nd	nd	nd	nd	nd	nd	nd
Ba	3.79	7.97	3.70	2.03	1.7	1.17	nd	nd	nd	nd	nd	nd	nd
Pb	0.405	31.1	30.3	15.6	19.0	7.77	1.25	*0.537*	bdl	bdl	1.54	3.80	1.93
Ti	1855	2549	843	31.0	54.4	nd	nd	nd	nd	nd	277766	301983	324416
Nb	0.150	0.135	bdl	bdl	bdl	bdl	404	363	896	819	318	135	112
Ta	0.030	0.017	bdl	bdl	bdl	bdl	31.1	24.7	69.5	57.7	26.7	10.6	7.66
Zr	2.10	21.7	3.11	bdl	0.196	0.161	59.2	28.7	24.9	22.7	16.1	23.2	11.4
Hf	0.300	0.971	*0.161*	bdl	bdl	bdl	3.77	1.87	1.65	1.38	1.97	1.51	0.944
P	nd	315	35.7	nd	bdl	bdl	bdl	bdl	bdl	bdl	386	152	245
La	0.044	448	0.305	1.24	35.9	17.9	bdl	bdl	bdl	bdl	1.20	5.69	1.78
Ce	0.094	1002	0.899	3.60	154	102	bdl	bdl	bdl	bdl	8.38	37.7	6.68
Nd	0.299	723	1.34	3.82	228	100	bdl	bdl	bdl	bdl	22.5	89.4	10.9
Sm	0.248	149	0.937	1.97	121	53.6	bdl	bdl	bdl	bdl	15.4	58.0	9.74
Eu	0.120	116	0.628	0.760	44.2	18.4	bdl	bdl	bdl	bdl	5.34	22.4	3.92
Yb	1.52	12.1	9.06	bdl	5.21	1.70	bdl	bdl	bdl	bdl	3.91	47.2	15.0
Y	12.1	317	59.4	1.53	78.4	40.2	bdl	0.131	*0.983*	bdl	95.4	411	171
Th	bdl	15.7	*0.026*	bdl	bdl	bdl	bdl	*0.122*	*0.105*	bdl	0.096	0.187	*0.079*
U	bdl	1.42	0.105	bdl	0.224	0.524	*0.111*	0.190	*0.053*	0.150	0.298	1.46	0.231
Nb/Ta							12.9	14.9	12.9	14.4	12.9	12.8	14.2
Zr/Hf							15.7	15.8	15.1	16.7	8.1	15.4	12.5

bdl = below detection limit: nd = not determined : italic numbers indicate maximum values.

eclogite host of the vein displays similar values for most trace elements, especially REE, than omphacite from the vein, the segregation or the eclogite host of the segregation. LILE, HFSE, and REE concentrations are higher in the cores than in the rims of matrix omphacite of the eclogite host of the vein (Table 4).

5.3.3. White mica

Two types of white mica—paragonite and phengite—are found in the segregation, but only paragonite occurs in the host eclogite (Table 1). In contrast, the vein contains only phengite, whereas the vein host eclogite has both phengite and paragonite. Phengite has a K_2O content of about 9 to 10 wt% and a Na_2O content of 0.6 to 0.9 wt%. The Si-contents cluster at 3.41 pfu in the segregation, 3.39 pfu in the vein and 3.29 to 3.33 pfu in the eclogite host of the vein (Table 3). Paragonite has a Na content of 0.7 to 0.8 pfu in the segregation and 0.6 to 0.8 pfu in the host eclogite. The micas display different trace element pattern, paragonite has higher Sr and LREE values than phengite (ca. 400–600 ppm Sr in paragonite vs. 50–100 ppm Sr in phengite), whereas phengite has a much higher concentration of Rb and Ba (200–250 ppm Rb and 1800–2000 ppm Ba in phengite vs. 3–7 ppm Rb and 67–100 ppm Ba in paragonite). Both kinds of mica have up to 3.5 to 4.0 ppm Pb (Table 4).

5.3.4. Amphibole

Glaucophane, barroisite, winchite, and hornblende occur in both the segregation and vein. Glaucophane is unzoned with Al^{IV} from 0.1 to 0.3 and $Na^{A\text{-site}} \leqslant 0.1$ pfu. Al^{VI} values range between 1.5 and 1.7 pfu. The Na_2O contents of sodic–calcic amphibole range between 3.7 and 5.1 wt%, those of calcic amphibole between 2.6 and 3.4 wt%. The texturally primary amphibole is glaucophane. Barroisite rims the glaucophane and omphacite of the eclogite hosts for both the segregation and the vein. The trace element values of the glaucophane are very low with most elements below 1 ppm. Barrosite has a slightly higher concentration than glaucophane (Table 4).

5.3.5. Zoisite

Zoisite occurs in the host eclogite of both the segregation and the vein, both as inclusions in garnet and as a matrix mineral. The Ps-content $[100 \times Fe^{3+}/(Al + Fe^{3+})]$ of zoisite inclusions in garnet (8.5 to 11.9) is less than that of matrix zoisite (12.6 to 14.4). Zoisite from the eclogite host of the vein contains a Y and REE concentration in the range of 100–1000 ppm and of U of 1.42 ppm, Th of 15.7 ppm and Pb of 31.7 ppm. Zoisite in the eclogite host of the segregation displays about two orders of magnitude lower concentrations. Zoisite from the eclogite host of the segregation contains 59.4 ppm Y and 9.1 ppm Yb and that from the eclogite host of the vein, an average of 317 ppm Y and 12.1 ppm Yb. However, zoisite from the eclogite host of the segregation contains 1775 ppm Sr and from the eclogite host of the vein 984 ppm Sr (Table 4).

5.3.6. Ankerite

Ankerite has XFe values from 0.13 to 0.16 in the segregation, from 0.15 to 0.20 in the vein and from 0.17 to 0.20 in eclogite host of the vein. Ankerite from the segregation, the vein and the eclogite host of the vein all similar trace element concentrations. Most trace elements are between 5 and 1 ppm (REE + Y) with higher values for Sr (1028 ppm) and Pb (15.6 ppm). The concentrations of the HFSE are less than the detection limit (Table 4).

5.3.7. Apatite

Apatite from both the segregation and its eclogite host has an average F content of 2.04 wt%; apatite from the vein displays an higher average F content of 2.36 wt% (Table 3). Cl is mostly below detection limits in the apatite analyses. Apatite in the vein and the eclogite host of the segregation contains high concentrations of almost all trace elements, exceptions are the HFSE which are below the detection limit. The apatite of the vein has two times higher concentrations than that of the host of the segregation, with e.g., 78.4 ppm vs. 40.2 ppm Y, 35.9 ppm vs. 17.9 ppm La, and 121 ppm vs. 53.6 ppm Sm (Table 4).

5.3.8. Rutile and titanite

The HFSE concentrations of rutile in the segregation and the vein are all similar to those of their host eclogites, but generally slightly lower. Rutile prisms exhibit no major and trace element zoning. Vein and host eclogite rutile have higher Nb and Ta contents (819 ppm Nb and 57.7 ppm Ta in the vein; 896 ppm Nb and 69.5 ppm Ta in the host eclogite) than rutile from the segregation and its host (363 ppm Nb and 24.7 ppm Ta; 404 ppm Nb and 31.1 ppm Ta, respectively). Rutile from the host eclogites contains more Zr and Hf than that of the segregation or the vein (59.2 ppm Zr and 3.77 ppm Hf in the host vs. 28.7 ppm Zr and 1.87 ppm Hf in its segregation; 24.9 ppm Zr and 1.65 ppm Hf in the host vs. 22.7 ppm Zr and 1.38 ppm Hf in its vein). The Nb/Ta ratios of the rutile in the segregation, vein and their host eclogite vary between 12.9 and 14.9 (14.9 for the segregation, 12.9 for the host of the segregation, 14.4 for the vein and 12.9 for the vein host eclogite). However, Zr/Hf ratios show a relatively narrow range, 15.8 for the segregation, 15.7 for the host of the segregation, 16.7 for the vein and 15.1 for the vein host eclogite (Table 4).

The Al_2O_3 contents of titanite ranges between 1.5 and 2.8 wt% and TiO_2 content between 34 and 39 wt%. Titanite in the eclogite host of the vein has 318 ppm Nb and 26.7 ppm Ta; that from the eclogite host of the segregation, 135 ppm Nb and 10.6 ppm Ta; that from the segregation 112 ppm Nb and 7.66 ppm Ta. Titanite from the eclogite host of the segregation displays the greatest Y and Yb contents, 411 ppm Y and 47.2 ppm Yb (Table 4).

6. DISCUSSION

6.1. Release and short-distance transport of Ti–Nb–Ta-bearing fluids

The large size of the acicular rutile crystals occurring in the segregation suggest unhindered growth from a Ti–Nb–Ta

supersaturated solution in an open, fluid filled cavity under hydrostatic conditions either as a result of P_{fluid} exceeding the least principal compressive stress (σ_3) by an amount greater than the tensile strength of the host rock (e.g., Brunsmann et al., 2000) or due to fluid coalescence to minimize the interfacial energy between fluid and minerals (e.g., Watson and Brenan, 1987). Local high fluid pressure may result from devolatilization during prograde metamorphism, which can induce hydraulic fracturing in the host rock (e.g., Yardley, 1986; Davies, 1999; Gao and Klemd, 2001). The prograde chemical zoning of garnet, its inclusions of the relict blueschist-facies mineral assemblage (paragonite, zoisite, glaucophane, and titanite), in combination with the replacement of titanite by rutile as observed in the host eclogite indicate that the eclogite underwent a dehydration process at the blueschist to eclogite transition, similar to that reported for other eclogites from the Tianshan subduction complex (Gao and Klemd, 2001). Reactions that were involved in the transformation of the volatile-rich blueschist to the volatile-poor eclogite are e.g.,:

$$2\text{Czo} + 5\text{Ttn} => 3\text{Grs} + 5\text{Rt} + 2\text{SiO}_2 + \text{H}_2\text{O} \quad (1)$$

$$6\text{Czo} + 13\text{Fe-Gln} = 9\text{Alm} + 26\text{Jd} + 12\text{Hed} + 19\text{Qtz} + 16\text{H}_2\text{O}, \quad (2)$$

$$\text{Fe-Gln} + \text{Pg} => \text{Alm} + 3\text{Jd} + 2\text{Qtz} + 2\text{H}_2\text{O}, \quad (3)$$

and

$$7\text{Pg} + 18\text{Ttn} + 3\text{Ank} = 5\text{Jd} + 7\text{Grs} + \text{Fe-Gln} + 18\text{Rt} + 6\text{CO}_2 + 6\text{H}_2\text{O}, \quad (4)$$

$$2\text{Fe-Gln} + 6\text{Ttn} + \text{Ank} = 4\text{Jd} + 7\text{Hed} + 6\text{Rt} + 2\text{H}_2\text{O} + 2\text{CO}_2 \quad (5)$$

$$26\text{Fe-Gln} + 12\text{Czo} + 19\text{Ank} = 52\text{Jd} + 43\text{Hed} + 18\text{Alm} + 38\text{CO}_2 + 32\text{H}_2\text{O} \quad (6)$$

if CO_2 is considered (e.g., Gao and Klemd, 2001; King et al., 2004; John et al., 2007). The primary low-salinity, aqueous fluid inclusions preserved in omphacite (Fig. 4a–c) are interpreted to represent relics of this fluid releasing process. The absence of kyanite and the presence of paragonite in the segregation and the host eclogite provide a maximum H_2O-dependent pressure of about ~1.9 GPa at 500 to 600 °C using the univariant reaction $\text{Pg} = \text{Omph}_{\text{Jd50}} + \text{Ky} + \text{H}_2\text{O}$. Temperature estimates were obtained by means of the garnet-clinopyroxene thermometer of Ellis and Green (1979) and the Zr-in-rutile thermometer of Watson et al. (2006). Temperatures range between 500 and 600 °C for the host eclogite at 1.9 GPa and 490 to 580 °C at 1.9 GPa for the segregation according to the Fe–Mg thermometry and are ca. 490 and ca. 480 °C, respectively, according to the Zr-in-rutile thermometry, indicating that the segregation formed under the same P–T conditions as the host eclogite. The fluid phase that is in equilibrium with the minerals in the host's of the segregation and vein shows a low X_{CO_2} of <0.007. This is demonstrated by T–X_{CO_2} calculations in the CaNaTiFASHC-endmember system for $0.001 < X_{CO_2} < 0.999$ and temperatures between 500 and 600 °C at a constant pressure of 1.9 GPa. These X_{CO_2} calculations were conducted with the internally consistent thermodynamic dataset of Holland and Powell (1990) with the endmembers grossularite, almandine, hedenbergite, jadeite, quartz, Fe–glaucophane, paragonite, ankerite, rutile, titanite, and an H_2O–CO_2 fluid (computer program Thermocalc v. 3.1, Powell and Holland, 1988). All of these phases were used to calculate an intersection of mineral-endmembers reactions at $X_{CO_2} = 0.0064$ at the relevant P–T conditions of 500–600 °C at 1.9 GPa. It was not possible to calculate such a concise X_{CO_2} for the segregation and the vein due to the absence of paragonite and/or zoisite (Table 1). Although the low X_{CO_2}, which was calculated for the fluid in equilibrium with the host rocks, is in accordance with the low CO_2 content in the primary fluid inclusion in omphacite of the host rocks and the segregation and vein as well (see above). However, the maximum density isochores pass about 1.1 GPa below these peak metamorphic conditions, which corresponds with isochores calculated forprimary inclusions in omphacite in eclogites from the same area (cf. Fig. 6 of Gao and Klemd, 2001). This indicates a modification of the fluid density due to re-equilibration during exhumation of the eclogites (see above). A mismatch between pressure estimates based on mineral geothermobarometry and fluid inclusion-derived isochores due to post peak metamorphic re-equilibration is commonly observed in eclogite-facies rocks (e.g., Klemd, 1989; Philippot and Selverstone, 1991; Klemd and Bröcker, 1999; Scambelluri and Philippot, 2001). However, although the density of fluid inclusions in the Tianshan high-pressure segregations and veins has been re-equilibrated during exhumation, the textural evidence constrains the entrapment of primary fluids during eclogite-facies conditions (see for detailed discussion Philippot and Selverstone, 1991; Selverstone et al., 1992; Gao and Klemd, 2001; Scambelluri and Philippot, 2001).

Garnet from the eclogite host of the segregation displays trace element zoning, with decreases of Ti, Nb, Ta, K, Rb, and Ba, and increases of Y and Yb from core to rim (Table 4). Omphacite in the eclogite host of the segregation also shows a similar trace element zoning to that of the garnet (Table 4). Increase of the Y and Yb concentrations from core to rim of garnet probably results from the prograde breakdown of REE-rich accessory phases (reaction 1), which contributed to the garnet trace element budget (King et al., 2004; Buick et al., 2006; John et al., 2007). Here, the titanite inclusion in a rutile grain (Fig. 3c) and the zoisite inclusions in garnet of the host eclogite (Fig. 3a) may indicate titanite- and zoisite-consuming reactions, such as the reaction 1. Both titanite and zoisite have high HREE concentrations (Table 4) and thus could release considerable amounts of Y and HREE while they are being consumed during mineral reactions, supplying Y and Yb for the rims of both garnet and omphacite (see also King et al., 2004, John et al., 2007). The large amounts of Ti–Nb–Ta as well as some of the Zr and Hf, which were released during the dissolution of titanite, were incorporated into the cm-sized rutile crystals in the segregation. However, most of the Zr and Hf were probably incorporated into the fine-grained zircons in the host eclogite. The modal amounts of titanite/rutile towards the segregation decrease significantly

over a distance of ten centimeters in the host eclogite, whereas the modal amount of rutile is always lower than that of (relict) titanite (Table 1).

The Ti, Nb, Ta, LILE, and HREE contents of the host eclogite decrease towards the segregation (Figs. 7 and 9), which suggests that these elements were mobilized. This is in accordance with the consumption of titanite during rutile-forming reactions and the occurrence of only minor relict paragonite and zoisite as inclusions in garnet 2 of the host eclogites. The decreasing Ti content towards the segregation of both matrix garnet rim and omphacite core in the host eclogite (Fig. 8) provides further evidence that Ti and coherent Nb and Ta were scavenged from the host rock during the dehydration of the blueschist to eclogite. This produces a depletion halo in the eclogite host, and Ti, Nb, and Ta enrichment in the segregation.

However, a mass balance calculation is required to determine whether the change in concentration of the trace elements is due to dilution or scavenging. This will further clarify whether there are systematic variations with respect to a geochemical frame, which might be otherwise covered by a metasomatic overall mass gain or loss. To discuss mass balance, an immobile geochemical frame has to be chosen (Ague, 2003a). This is complicated due to the heterogeneous bulk chemistry and mineral distribution in the host eclogite. In the present study, we used the average host rock as the *reference* rock and the samples along the profile were used for the mass balance calculation in order to obtain information on elemental loss or gain through the blueschist to eclogite transition. A "graphical" approach was used to obtain the geochemical reference frame to discuss the trace element mobilization (Fig. 9). Zr and Hf were chosen as immobile elements because the existence of fine-grained zircons in the host and the absence in the segregation also suggest that both Zr and Hf were almost immobile during the dehydration of the host eclogites. In addition, the Zr/Hf ratio of the host rocks varies from 35 to 37, within the range typical for oceanic basalts. This also suggests that Zr and Hf were immobile. Their r_{inv} value for Zr and Hf ($C_i^{\text{altered rock}}/C_i^{\text{precursor}}$; Ague, 2003a) is about 0.93 for (a), 1.01 for (b), 1.22 for (c), 1.37 for (d), and 1.53 for (e). The r_{inv} value of 0.93 indicates an overall rock mass gain

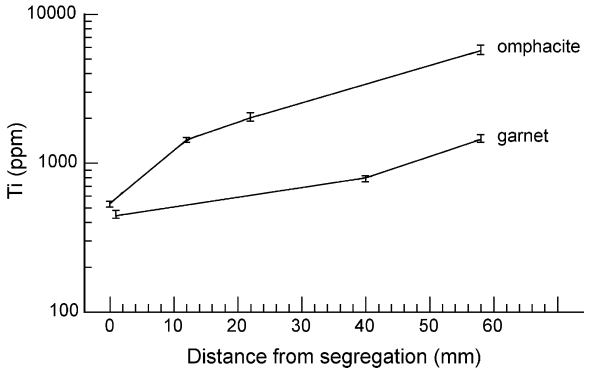

Fig. 8. Titanium contents of garnet 2 and omphacite along a profile in the host eclogite showing a decrease towards the segregation. Data are measured with LA-ICP MS and are shown in Table 4.

~8% (a). (b) shows evidence for a constant mass (1% mass gain), whereas the overall rock mass loss of (c) is ~20%, of (d) ~30%, and of (e) 35%, indicating that the mass loss increases towards the segregation. Relative to the r_{inv} values, almost all other elements display a mass loss (Fig. 10). Nb, Ta, and Ti were mobilized during the dehydration of the host and fractionated from Zr and Hf. Significant losses of LILE, Nb, Ta, and Ti (~75% to ~5% for (e)) demonstrate that Ti–Nb–Ta, together with LILE and Sr were locally mobilized into the segregation. The calculated loss of Nb, Ta, and Ti and LILE gradually increases towards the segregation (from ~20% to ~25% for (b), ~45% to ~55% for (c), ~50% to ~65% for (d), and ~70% to ~75 for (e)), indicating that these elements were more efficiently scavenged closer to the segregation (Fig. 10). Th and U show a loss of ~40% (b) to ~65% for (e), similar to that of the LREE with ~45% (b) and ~70% (e). However, HREE and Y remain constant up to the sample (b) and then a mass loss of ~65% towards (e) is calculated. For major elements, the mass loss of Si, Al, Fe, and Ca (~34% to ~60%) is greater than that of Na (~20%). P shows a trend of decreasing mobilization towards the segregation, whereas, Mg was comparatively immobile, when examined in the reference frame of Zr and Hf. During dehydration, Ti, Nb, Ta, LILE, and REE were all efficiently mobilized into the segregation (Fig. 10).

6.2. Relatively long-distance transport of Ti–Nb–Ta-bearing fluids

The temperatures calculated for the peak of eclogite facies metamorphism of the vein's eclogite host is 475–590 °C at 1.9 GPa for Fe–Mg exchange thermometry and ca. 540 °C for Zr-in-rutile thermometry. Pressure estimates, which are based on the phengite-barometry (Waters and Martin, 1993), confirm a maximum pressure of 1.9 GPa for the host eclogite. Temperature estimates for the vein of ca. 525 °C were obtained by Zr-in-rutile thermometry only. The modal abundance of the minerals stay constant towards the vein and no evidence for mineral reactions or textural changes indicative of fluid-rock interaction processes are present in the host eclogite and at the interface between host and vein. The sharp interfaces between the rutile-bearing vein TS9-4 and its host eclogite and the cross-cutting relation between vein and host indicate brittle behavior of the eclogite host and an external source for the fluid from which this 'transport vein' precipitated (Bons, 2001; John et al., 2007). The centimeter-sized rutile prisms, fibrous omphacite in the vein and aqueous fluid inclusions in omphacite suggest that a Ti-enriched aqueous fluid phase formed the vein minerals.

The minerals of the rutile-bearing vein show evidence for precipitation from a fluid, which appears to have originated at some distance (externally) from the present host eclogite. The precursor rocks of the investigated samples (hosts of the segregation and the vein) probably formed in different tectonic settings and were juxtaposed during the subduction process. Considering that rutile-bearing segregations are very common in the Tianshan vein system (Fig. 2), we speculate that the vein forming fluid may stem from a source

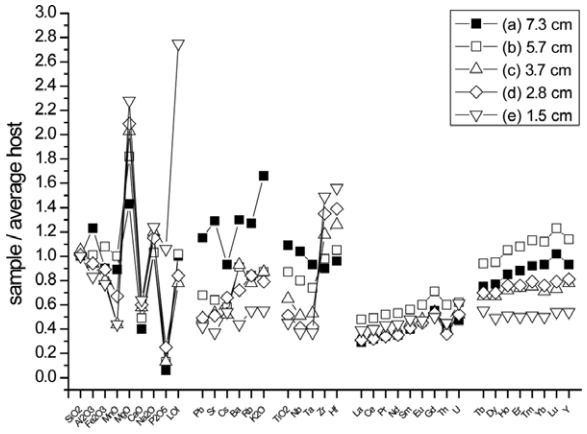

Fig. 9. Normalized concentration diagram (normalized to the average host of the segregation) showing the variations of the trace element composition along the profile towards the host. Note that most trace elements decrease whereas Zr and Hf increase in their concentrations.

such as the depletion halo surrounding the segregation. Because the vein is more than ten meters long, the fluid must have been transported along the channel (fracture) over a distance of at least ten meters. When considering the ubiquitous occurrences of the rutile-bearing veins, with their rather characteristic and uniform mineral assemblage, cutting through different lithologies (Fig. 2) a transport of more than several tens of meters seems to be even more likely. It's a reasonable assumption that such vein systems may represent the pathways of fluid flow through and out of the slab (John et al., 2007). In this regard, it should be pointed out that previous fluid inclusion studies revealed—by the preservation of primary, heterogeneous fluid inclusion populations—that large fluid activity gradients could persist during eclogite-facies conditions as a consequence of local fluid production and/or buffering as well as limited fluid flow at depth >60 km in a subduction zone (e.g., Philippot and Selverstone, 1991; Selverstone et al., 1992; Klemd et al., 1992; Franz et al., 2001). Clearly, this is not the case in the here investigated homogeneous, primary fluid inclusion population in omphacite (cf., Gao and Klemd, 2001). In addition, the preservation of small scale isotopic heterogeneities in eclogites led Scambelluri and Philippot (2001) to suggest that fluids (and trace elements) mostly remain entrapped in the subducting rocks within subduction zones and are released into the deep mantle at depth greater than those revealed by most exposed eclogites (cf. Brenan et al., 1995). The isolation of H_2O- and CO_2-rich fluids in eclogites prevents—due to their large dihedral angle—any large-scale fluid flow along the grain boundaries (e.g., Watson and Brenan, 1987; Mibe et al., 2003). Consequently, the transport of aqueous fluid and thereby trace elements from the slab into the overlying mantle wedge, can be achieved only by focused fluid flow along hydrofractures and shear zones (cf., Davies, 1999; Zack and John, 2007) and, thus, this process cannot be resolved by fluid inclusion or isotope studies on undeformed and unveined eclogites (for an extensive discussion see Klemd, 2004).

6.3. Implications for subduction-zone fluids

In most eclogite-facies metabasites, rutile is the stable titanium-phase. It is thought to prevent almost the entire HFSE-contents of subducted MORB from being mobilized by aqueous fluids (e.g., Rudnick et al., 2000; Zack et al., 2002). This implies that during dehydration reactions a

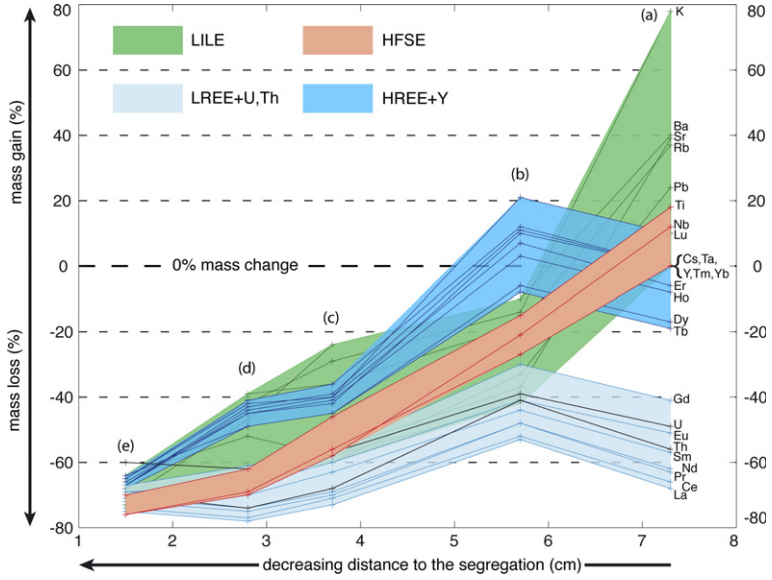

Fig. 10. Concentration ratio diagram illustrating the mass loss of the segregation host eclogite (sample TS33-5B). Estimate of the concentration ratio for immobile elements (r_{inv}) indicated by the thick horizontal dashed line, which is marked by 0% mass change. With respect to the geochemical frame (Zr and Hf) all other trace elements behave mobile and are scavenged from the host into the segregation. The trace elements behave rather similar within groups, such as LILE, HFSE, LREE + U, Th, and HREE + Y. Major elements are not shown for clarity reasons.

HFSE-depleted aqueous fluid forms, which may be responsible for the negative Nb anomaly in arc lavas (e.g., Zack et al., 2002). The low experimental solubility of Ti–Nb–Ta in subduction zone fluids (Audetat and Keppler, 2005; Tropper and Manning, 2005) supports this suggestion. However, in some cases (e.g., Sorensen and Grossman, 1989; Brunsmann et al., 2000; Bröcker and Enders, 2001; Rubatto and Hermann, 2003; John et al., 2007) HFSE appear to have been mobile during subduction zone metamorphism. Van Baalen (1993) has emphasized that the solubility of rutile was probably significant under eclogite-facies conditions, yet the transport of Ti seems to have been limited to a centimeter scale at Monviso (Philippot and Selverstone, 1991) and over meters in the Catalina amphibolite unit (Sorensen and Grossman, 1989). In the present study, the trace element depletion halo of the segregation host eclogite demonstrates that LILE and Ti–Nb–Ta and minor REE were mobilized on the centimeter-scale by an aqueous fluid, which itself was liberated by the dehydration of subducted oceanic basalts. Furthermore, the rutile-bearing vein indicates that Ti–Nb–Ta can be mobilized in solution and transported, at least over a distance of several meters but probably over a much longer distance considering the rutile-bearing vein system. Experimental results show that fluoride complexes significantly enhance the solubility of TiO_2 (Bright and Readey, 1987; Van Baalen, 1993) and dissolved albite in fluids also increases the rutile solubility pointing to F^- and Na–Al–Si polymers as potential complex former (e.g., Antignano and Manning, 2005). Fluorine-rich apatite in the segregation, its host eclogite and the vein indicates that the fluid had an elevated F-content (Brenan, 1993). The newly formed omphacites (with a high jadeite component [$NaAlSi_2O_6$]) within the depletion halo of the segregation, the relic albite ($NaAlSi_3O_8$) in the core and the NaCl-dominated primary fluid inclusions in the fibrous-vein omphacite indicate that significant amounts of Na, Si, and Al were in solution (Manning, 1998; John et al., 2007). It is thus reasonable to assume that F, possibly in combination with aqueous Na-aluminosilicate polymers probably enhanced the Ti–Nb–Ta solubilities in these fluids (Manning, 2004; John et al., 2007) and thus may have been responsible for keeping Ti–Nb–Ta in solution.

The petrological and structural observations gathered from the segregation and the vein suggest a fluid and element transport into and along (hydraulic) fractures (Brunsmann et al., 2000; Bons, 2001; Ague, 2003b; John et al., 2007; Zack and John, 2007). The original fluid unloaded Ti–Nb–Ta by means of rutile precipitation (Fig. 1d). The texture of rutile needles immersed in ankerite in the segregation, the carbonate crystals in primary fluid inclusions in fibrous omphacite, and the presence of ankerite in the vein suggest gradients of X_{CO_2} (e.g., Molina et al., 2004). This assumption is supported by the observed carbonate inclusions in garnets, indicating that reactions 5 and 6 liberated CO_2 into the fluid during eclogitization. The addition of CO_2 to H_2O-rich fluids can cause the precipitation of rutile, because it reduces its solubility (Ayers and Watson, 1993). The precipitation of rutile in segregations and vein fillings, will leave a relatively Ti–Nb–Ta depleted residual fluid. Furthermore, the absence of large modal amounts of LILE- or REE- carrying minerals, such as micas and epidote-minerals in the segregation and the vein suggest that some fluid has escaped from the cavity and fracture, thereby draining LILE and REE. Fluids rich in REE and LILE and poor in HSFE satisfy basic characteristics typical for the slab signature of arc magmas. The decoupling of Zr and Hf from Nb, Ta, and Ti may be caused by the growth of fine-grained zircons in the host rocks, which did not occur in the segregation and vein. Thus, mainly titanite but also some rutile were involved within the blueschist-dehydration process and consequently dissolved, whereas during these *in situ* processes (i.e., segregation formation) zircon remained stable.

7. CONCLUSIONS

1. Petrological and geochemical data indicate that Ti, Nb, and Ta were coherently mobilized and scavenged by an aqueous fluid, which was probably liberated during the dehydration of the segregation host. The dissolution of titanite in the eclogite released Ti–Nb–Ta, which were deposited in the segregation after transport on a centimeter scale. This transport is ascribed to the presence of F^- and Na-aluminosilicate polymers in the fluid, which probably enhanced Ti–Nb–Ta solubilities.
2. A mass balance calculation of the altered host eclogite indicates that a LILE, Ti–Nb–Ta and REE depletion halo formed around the segregation. About 65% to 75% of these elements were scavenged from the host eclogite.
3. The sharp interfaces between the centimeter-sized rutile-bearing vein and the host eclogite, as well as the lack of any evidence for fluid-rock interaction in the host, indicate that a Ti–Nb–Ta-enriched aqueous fluid phase, with an external source, was transported over a distance of at least several meters. However, the ubiquitous occurrence of the rutile-bearing veins suggest a transport of more than several tens of meters.
4. The decoupling of Nb, Ta, and Ti from Zr and Hf most likely occurred because zircon grains remained unaffected or were dissolved by fluids generated by *in situ* dehydration reactions.
5. During the transport of fluids to an open cavity (now filled with the segregation minerals) or along hydraulic fractures (now filled by vein minerals), the original fluid unloaded some Ti–Nb–Ta by means of rutile precipitation. The variations of X_{CO_2} in the aqueous fluids during prograde metamorphism may have caused the precipitation of rutile.
6. The abundant rutile-bearing segregations and veins in the high-pressure belt of the Tianshan Mts. suggest that the here described process of fluid and trace element release combined with element fractionation may play a significant role in the generation of subduction zone fluids that finally may flux the mantle wedge to produce magma with an arc signature.

ACKNOWLEDGEMENTS

This research was supported by 'National Basic Research Program of China' (2007CB411302 and 2001CB409803), National Natural Science Foundation of China (40421202), 'Funds for

Hundred Outstanding Talents Plan' sponsored by Chinese Academy of Sciences, and the Deutsche Forschungsgemeinschaft (KL 692/17-2). We thank R. Baur, H. Brätz, and U. Westernströer for help with the XRF and LA-ICP-MS analyses, G. M. Shu for electron microprobe analyses. The authors appreciate the constructive comments of S. Sorensen on an earlier version of this manuscript. Detailed and constructive reviews by J. M. Brenan, M. D. Feineman, and C. E. Manning are gratefully acknowledged. Furthermore, we thank F. J. Ryerson for his editorial handling and comments. This publication is contribution No. 97 of the Sonderforschungsbereich 574 "Volatiles and Fluids in Subduction Zones" at Kiel University.

REFERENCES

Ague J. J. (2003a) Fluid infiltration and transport of major, minor, and trace elements during regional metamorphism of carbonate rocks, Wepawaug Schist, Connecticut, USA. *Am. J. Sci.* **303**, 753–816.

Ague J. J. (2003b) Fluid flow in the deep crust. *Treat. Geochem.* **3**, 195–228.

Antignano A. and Manning C. E. (2005) Rutile solubility in H_2O–$NaAlSiO_3$ fluids at high T and P: implications from HFSE mobility in subduction zones. *Eos Trans. AGU*, 85 (52), Fall Meet. Suppl. (abstr.) V31C-0620.

Armstrong J. (1995) CITZAF: a package of correction programs for the quantitative electron microbeam X-ray analysis of thick polished materials, thin films, and particles. *Microbeam Anal.* **4**, 177–200.

Audetat A. and Keppler H. (2005) Solubility of rutile in subduction zone fluids, as determined by experiments in the hydrothermal diamond anvil cell. *Earth Planet. Sci. Lett.* **232**, 393–402.

Ayers J. C. (1998) Trace element modeling of aqueous-peridotite interaction in the mantle wedge of subduction zones. *Contrib. Mineral. Petrol.* **132**, 390–404.

Ayers J. C. and Watson E. B. (1993) Rutile solubility and mobility in supercritical aqueous fluids. *Contrib. Mineral. Petrol.* **114**, 321–330.

Bakker R. J. (2003) Package Fluids 1. Computer programs for analysis of fluid inclusion data and for modeling fluid properties. *Chem. Geol.* **194**, 3–23.

Becker H., Jochum K. P. and Carlson R. W. (1999) Constraints from high-pressure veins in eclogites on the composition of hydrous fluids in subduction zones. *Chem. Geol.* **160**, 291–308.

Bons P. D. (2001) The formation of large quartz veins by rapid ascent of fluids in mobile hydrofractures. *Tectonophysics* **336**, 1–27.

Brätz H. and Klemd R. (2002) Analysis of rare earth elements in geological samples by Laser Ablation-Inductively Coupled Plasma Mass Spectrometry (LA-ICP-MS). Online publication: No 5988-6305EN, Agilent Technologies.

Brenan J. M. (1993) Partitioning of fluorine and chlorine between apatite and aqueous fluids at high pressure and temperature: implications for the F and Cl content of high *P–T* fluids. *Earth Planet. Sci. Lett.* **117**, 251–263.

Brenan J. M., Shaw H. F., Phinney D. L. and Ryerson F. J. (1994) Rutile-aqueous fluid partitioning of Nb, Ta, Hf, Zr, U and Th: implications for high field strength element depletions in island-arc basalts. *Earth Planet. Sci. Lett.* **128**, 327–339.

Brenan J. M., Shaw H. F., Ryerson F. J. and Phinney D. L. (1995) Mineral-aqueous fluid partitioning of trace elements at 900 °C and 2.0 Gpa: constraints on the trace element chemistry of mantle and deep fluids. *Geochim. Cosmochim. Acta* **59**, 3331–3350.

Bright E. and Readey D. W. (1987) Dissolution kinetics of TiO_2 in HF–HCl solutions. *J. Am. Ceram. Soc.* **70**, 900–906.

Bröcker M. and Enders M. (2001) Unusual bulk-rock compositions in eclogite-facies rocks from Syros and Tinos (Cyclades, Greece): implications for U–Pb zircon geochronology. *Chem. Geol.* **175**, 581–603.

Brunsmann A., Franz G., Erzinger G. and Landwehr D. (2000) Zoisite- and clinozoisite-segregation in metabasites (Tauern Window, Austria) as evidence for high-pressure fluid-rock interaction. *J. Metamorph. Geol.* **18**, 1–21.

Buick I. S., Hermann J., Williams I. S., Gibson R. L. and Rubatto D. (2006) A SHRIMP U–Pb and LA-ICP-MS trace element study of the petrogenesis of garnet–cordierite–orthoamphibole gneisses from the Central Zone of the Limpopo Belt, South Africa. *Lithos* **88**, 150–172.

Davies J. H. (1999) The role of hydraulic fractures and intermediate depth earthquakes in generating subduction-zone magmatism. *Nature* **398**, 142–145.

Ellis D. J. and Green D. H. (1979) An experimental study of the effect of Ca upon garnet-clinopyroxene Fe–Mg exchange equilibria. *Contrib. Mineral. Petrol.* **71**, 13–22.

Feineman M. D., Ryerson F. J., DePaolo D. J. and Plank T. (2007) Zoisite-aqueous fluid trace element partitioning with implications for subduction zone fluid composition. *Chem. Geol.* **239**, 250–265.

Franz L., Romer R. L., Klemd R., Schmid R., Oberhänsli R., Wagner T. and Dong S. (2001) Eclogite-facies quartz veins within metabasites of the Dabie Shan (eastern China); pressure-temperature-time-deformation path, composition of the fluid phase and fluid flow during exhumation of high-pressure rocks. *Contrib. Mineral. Petrol.* **141**, 322–346.

Gao J., He G., Li M., Xiao X., Tang Y., Zhou M. and Wang J. (1995) The mineralogy, petrology, metamorphic *P–T–D–t* trajectory and exhumation mechanism of blueschists, south Tianshan, northwestern China. *Tectonophysics* **250**, 151–168.

Gao J., Li M., He G., Xiao X. and Tang Y. (1998) Paleozoic tectonic evolution of the Tianshan orogenic belt northwest China. *Tectonophysics* **287**, 213–231.

Gao J., Klemd R., Zhang L., Wang Z. and Xiao X. (1999) *P–T* path of high pressure-low temperature rocks and tectonic implications in the western Tianshan Mountains (NW China). *J. Metamorph. Geol.* **17**, 621–636.

Gao J. and Klemd R. (2001) Primary fluids entrapped at blueschist to eclogite transition: evidence from the Tianshan metasubduction complex in northwestern China. *Contrib. Mineral. Petrol.* **142**, 1–14.

Gao J. and Klemd R. (2003) Formation of HP-LT rocks and their tectonic implications in the western Tianshan Orogen, NW China: geochemical and age constraints. *Lithos* **66**, 1–22.

Garbe-Schönberg C. D. (1993) Simultaneous determination of thirty-seven trace elements in twenty-eight international rock standards by ICP-MS. *Geostandard. Newsl.* **17**, 81–97.

Goldstein R. H. and Reynold T. J. (1994) Systematics of fluid inclusions in diagenetic minerals. *SEPM Short Course* **31**, 199.

Heinrich W. and Gottschalk M. (1995) Metamorphic reaction between fluid inclusions and mineral host I: progress of the reaction calcite + quartz = wollastonite + CO_2 in natural wollastonite-host fluid inclusions. *Contrib. Mineral. Petrol.* **122**, 51–61.

Hermann J., Spandler C., Hack A. and Korsakov A. V. (2006) Aqueous fluids and hydrous melts in high-pressure and ultrahigh pressure rocks: implications for element transfer in subduction zones. *Lithos* **92**, 399–417.

Holland T. J. B. and Powell R. (1990) An internally consistent thermodynamic data set with uncertainties and correlations: the system K_2O–Na_2O–CaO–MgO–MnO–FeO–Fe_2O_3–Al_2O_3–TiO_2–SiO_2–C–H_2–O_2. *J. Metamorph. Geol.* **8**, 89–124.

Jochum K. P., Stoll B., Herwig K., Willbold M. and Hofmann A. W., et al. (2006) MPI-DING reference glasses for in-situ microanalysis: new reference values for element concentrations and isotope ratios. *Geochem. Geophys. Geosyst.* **7**, Q02008. doi:10.1029/2005GC001060.

John T. and Schenk V. (2003) Partial eclogitisation of gabbroic rocks in a late Precambrian subduction zone (Zambia): prograde metamorphism triggered by fluid infiltration. *Contrib. Mineral. Petrol.* **146**, 174–191.

John T., Scherer E. E., Haase K. M. and Schenk V. (2004) Trace element fractionation during fluid-induced eclogitization in a subducting slab: trace element and Lu–Hf–Sm–Nd isotope systematics. *Earth Planet. Sci. Lett.* **227**, 441–456.

John T. and Schenk V. (2006) Interrelations between intermediate-depth earthquakes and fluid flow within subducting oceanic plates: constraints from eclogite-facies pseudotachylytes. *Geology* **34**, 557–560.

John T., Klemd R., Gao J. and Garbe-Schönberg C. D. (2007) Trace-element mobilization in slabs due to, non-steady-state fluid-rock interaction: constraints from an eclogite-facies transport vein in blueschist (Tianshan, China). Lithos, in press, doi:10.1016/j.lithos.2007.09.005.

Kessel R., Schmidt M. W., Ulmer P. and Pettke T. (2005) Trace element signature of subduction-zone fluids, melts and supercritical liquids at 120–180 km depth. *Nature* **437**, 724–727.

King R. L., Bebout G. E., Kobayashi K., Nakamura E. and van der Klauw S. N. G. C. (2004) Ultrahigh-pressure metabasaltic garnets as probes into deep subduction zone chemical cycling. *Geochem. Geophys. Geosyst.* **5**, Q12J14. doi:10.1029/2004GC000746.

Klemd R. and Bröcker M. (1999) Fluid influence on mineral reactions in ultrahigh-pressure granulites: a case study in the Snieznik Mts. (West Sudetes, Poland). *Contrib. Mineral. Petrol.* **136**, 358–373.

Klemd R., van den Kerkhof A. M. and Horn E. E. (1992) High-density CO_2–N_2 inclusions in eclogite-facies metasediments of the Münchberg gneiss complex, SE Germany. *Contrib. Mineral. Petrol.* **11**, 409–441.

Klemd R. (1989) *P–T* evolution and fluid inclusion chracteristics of retrograded eclogites, Münchberg gneiss complex, Germany. *Contrib. Mineral. Petrol.* **102**, 221–229.

Klemd R. (2004) Fluid inclusions in epidote minerals and fluid development in epidote-bearing rocks. *Rev. Mineral. Geochem.* **56**, 197–234.

Klemd R., Bröcker M., Hacker B. R., Gao J. and Gans P. (2005) New age constraints on the metamorphic evolution of the high-pressure/low-temperature Belt in the Western Tianshan Mountains, NW China. *J. Geol.* **113**, 157–168.

Klemd R., Schröter F., Will T. and Gao J. (2002) *P–T*-evolution of glaucophane-clinozoisite bearing HP-LT rocks in the western Tianshan orogen, NW China. *J. Metamorph. Geol.* **20**, 239–254.

Kretz R. (1983) Symbols for rock-forming minerals. *Am. Mineral.* **68**, 277–279.

Manning C. E. (1998) Fluid compostion at the blueschist-eclogite transition in the model system Na_2O–MgO–Al_2O_3–SiO_2–H_2O–HCl. *Schweiz. Mineral. Petrogr. Mitt.* **78**, 225–242.

Manning C. E. (2004) The chemistry of subduction-zone fluids. *Earth Planet. Sci. Lett.* **223**, 1–16.

McCulloch M. T. and Gamble A. J. (1991) Geochemical and geodynamical constraints on subduction zone magmatism. *Earth Planet. Sci. Lett.* **102**, 358–374.

Mibe K., Yoshino T., Ono S., Yasuda A. and Fujii T. (2003) Connectivity of aqueous fluid in eclogite and its implications for fluid migration in the Earth's interior. *J. Geophys. Res.* **108**, 2295–3006.

Molina J. F., Poli S., Austrheim H., Glodny J. and Rusin A. (2004) Eclogite-facies vein systems in the Marun-Keu complex (Polar Urals,Russia): textural, chemical and thermal constraints for patterns of fluid flow in the lower crust. *Contrib. Mineral. Petrol.* **147**, 484–504.

Peacock S. M. (1993) The importance of blueschist → eclogite dehydration reactions in subducting oceanic crust. *Geol. Soc. Am. Bull.* **105**, 684–694.

Pfänder J. A., Münker C., Stracke A. and Mezger K. (2007) Nb/Ta and Zr/Hf in ocean island basalts—implications for crust–mantle differentiation and the fate of Niobium. *Earth Planet. Sci. Lett.* **245**, 158–172.

Philippot P. and Selverstone J. (1991) Trace-element-rich brines in eclogitic veins: implications for fluid composition and transport during subduction. *Contrib. Mineral. Petrol.* **106**, 417–430.

Powell R. and Holland T. J. B. (1988) An internally consistent thermodynamic data set with uncertainties and correlations: 3. Applications to geobarometry, worked examples and a computer program. *J. Metamorph. Geol.* **6**, 173–204.

Rubatto D. and Hermann J. (2003) Zircon formation during fluid circulation in eclogites (Monviso, Western Alps): Implications for Zr and Hf budget in subduction zones. *Geochim. Cosmochim. Acta* **67**, 2173–2187.

Rudnick R. L., Barth M., Horn I. and McDonough W. F. (2000) Rutile-bearing refractory eclogites; missing link between continents and depleted mantle. *Science* **287**, 278–281.

Ryerson F. J. and Watson E. B. (1987) Rutile saturation in magmas: implications for Ti–Nb–Ta depletion in island-arc basalts. *Earth Planet. Sci. Lett.* **86**, 225–239.

Schulz B., Bombach K., Pawlig S. and Brätz H. (2004) Neoproterozoic to Early-Palaeozoic magmatic evolution in the Gondwana-derived Austroalpine basement to the south of the Tauern Window (Eastern Alps). *Int. J. Earth Sci.* **93**, 824–843.

Scambelluri M. and Philippot P. (2001) Deep fluids in subduction zones. *Lithos* **55**, 213–227.

Scambelluri M., Bottazzi P., Trommsdorff V., Vannucci R., Hermann J., Gomez P. M. T. and Lopez S. V. V. (2001) Incompatible element-rich fluids released by antigorite breakdown in deeply subducted mantle. *Earth Planet. Sci. Lett.* **192**, 457–470.

Schmidt M. W. and Poli S. (1998) Experimentally based water budgets for dehydrating slabs and consequences for arc magma generation. *Earth Planet. Sci. Lett.* **163**, 361–379.

Selverstone J., Franz G., Thomas S. and Getty S. (1992) Fluid variability in 2 GPa eclogites as an indicator of fluid behaviour during subduction. *Contrib. Mineral. Petrol.* **112**, 341–357.

Sorensen S. S. and Grossman J. N. (1989) Enrichment of trace elements in garnet amphibolites from a paleo-subduction zone: Catalina Schist, southern California. *Geochim. Cosmochim. Acta* **53**, 3155–3177.

Stalder R., Foley S. F., Brey G. P. and Horn I. (1998) Mineral-aqueous fluid partitioning of trace elements at 900–1200 °C and 3.0–5.7 GPa: new experimental data for garnet, clinopyroxene, and rutile, and implications for mantle metasomatism. *Geochim. Cosmochim. Acta* **62**, 1781–1801.

Stolper E. and Newman S. (1994) The role of water in the petrogenesis of Mariana trough magmas. *Earth Planet. Sci. Lett.* **121**, 293–325.

Sun S. S. and McDonough W. F. (1989) Chemical and isotopic systematics of oceanic basalts: implications for mantle composition and processes. In *Magmatism in the Ocean Basin* (eds. A. D. Saunders and M. J. Norry), pp. 313–345. Magmatism in the Ocean Basin. Geol. Soc. Sp. Pub..

Sylvester P. J. (2003) Trace element analysis of fused whole rock glasses by laser ablation ICPMS. In Laser-Ablation ICPMS in the Earth Sciences. Principles and Applications (ed. Sylvester,

P. J.). Mineralogical Association of Canada Short Course Series 29, pp. 147–162.

Tatsumi Y. (1989) Migration of fluid phases and genesis of basalt magmas in subduction zones. *J. Geophys. Res.* **94**, 4697–4707.

Tropper P. and Manning C. E. (2005) Very low solubility of rutile in H_2O at high pressure and temperature, and its implications for Ti mobility in subduction zone. *Am. Mineral.* **90**, 502–505.

Van Baalen M. R. (1993) Titanium mobility in metamorphic systems: a review. *Chem. Geol.* **110**, 233–249.

Waters D. J. and Martin H. N. (1993) Geobarometry of phengite-bearing eclogites. *Terra Abstr.* **5**, 410–411.

Watson E. B. and Brenan J. M. (1987) Fluids in the lithosphere, 1. Experimentally-determined wetting characteristics of CO_2–H_2O fluids and their implications for fluid transport, host-rock physical properties, and fluid inclusion formation. *Earth Plant. Sci. Lett.* **85**, 497–515.

Watson E. B., Wark D. A. and Thomas J. B. (2006) Crystallization thermometers for zircon and rutile. *Contrib. Mineral. Petrol.* **151**, 413–433.

Wei C. J., Powell R. and Zhang L. F. (2003) Eclogites from the south Tienshan, NW China: petrological characteristic and calculated mineral equilibria in the Na_2O–CaO–FeO–MgO–Al_2O_3–SiO_2–H_2O system. *J. Metamorp. Geol.* **21**, 163–179.

Yardley B. W. D. (1986) Fluid migration and veining in the Connemara schists, Ireland. In *Fluid-Rock Interactions During Metamorphism* (eds. J. V. Walther and B. J. Wood). Springer-Verlag, pp. 109–131.

Zack T., Foley S. F. and Rivers T. (2002) Equilibrium and disequilibrium trace element partitioning in hydrous eclogites (Trescolmen, Central Alps). *J. Petrol.* **43**, 1947–1974.

Zack T. and John T. (2007) An evaluation of reactive fluid flow and trace element mobility in subducting slabs. *Chem. Geol.* **239**, 199–216.

Associate editor: F. J. Ryerson